Open access • Journal Article • DOI:10.1093/CVR/CVAA142

Deletion of fibroblast activation protein provides atheroprotection. — Source link

Sokrates Stein, Julien Weber, Stefanie Nusser-Stein, Jürgen Pahla ...+12 more authors

Institutions: University of Zurich, University of Sydney, university of lille, ETH Zurich

Published on: 21 Mar 2021 - Cardiovascular Research (Oxford University Press)

Topics: Fibroblast activation protein, alpha, Sirius Red and Fibrous cap

Deletion of fibroblast activation protein provides atheroprotection 1 2

Sokrates Stein, Julien Weber, Stefanie Nusser-Stein, Jürgen Pahla, Hui Zhang, Shafeeq Mohammed, Sara Oppi, Daniel Gaul, Francesco Paneni, Anne Tailleux, et al.

Deletion of fibroblast activation protein provides atheroprotection

Sokrates Stein[1,2]*, Julien Weber[1], Stefanie Nusser-Stein[1], Jürgen Pahla[1], Hui E. Zhang[3], Shafeeq A. Mohammed[1], Sara Oppi[1], Daniel S. Gaul[1], Francesco Paneni[1,2,4], Anne Tailleux[5], Bart Staels[5], Ferdinand von Meyenn[6], Frank Ruschitzka[2], Mark D. Gorrell[3], Thomas F. Lüscher[1,7], Christian M. Matter[1,2,*]

Affiliations

[1]Center for Molecular Cardiology, University of Zurich, CH-8952 Schlieren, Switzerland.

[2]Department of Cardiology, University Heart Center Zurich, University Hospital Zurich, CH-8091 Zurich Switzerland.

[3]Centenary Institute, The University of Sydney, Faculty of Medicine and Health, Sydney NSW 2050, Australia.

[4]Department of Research and Education, University Hospital Zurich, CH-8091 Zurich Switzerland.

[5]University of Lille, Inserm, CHU Lille, Institut Pasteur de Lille, U1011 - EGID, Lille, France.

[6]Institute of Food, Nutrition and Health, ETH Zurich, 8603 Schwerzenbach, Switzerland.

[7]Cardiology, Royal Brompton & Harefield Hospital Trust and Imperial College London, London SW3 6NP, United Kingdom.

***Addresses for correspondence**

Sokrates Stein, Center for Molecular Cardiology, University of Zurich, Wagistrasse 12, 8952 Schlieren, Switzerland. E-mail: sokrates.stein@uzh.ch. Phone: +41 44 635 5094.

Christian M. Matter, Center for Molecular Cardiology, University of Zurich, and Department of Cardiology, University Heart Center, University Hospital Zurich. Switzerland. E-mail: christian.matter@usz.ch. Phone: +41 44 255 3871.

Short title: Fibroblast activating protein deletion protects against atherosclerosis

Category: Original article

Word count: 5800

Abstract

Aims. Fibroblast activation protein (FAP) is upregulated at sites of tissue remodelling including chronic arthritis, solid tumours, and fibrotic hearts. It has also been associated with human coronary atherosclerotic plaques. Yet, the causal role of FAP in atherosclerosis remains unknown. To investigate the cause-effect relationship of endogenous FAP in atherogenesis, we assessed the effects of constitutive *Fap* deletion on plaque formation in atherosclerosis-prone *apolipoprotein E* (*Apoe*) or *low-density lipoprotein receptor* (*Ldlr*) knockout mice.

Methods and results. Using *en face* analyses of thoraco-abdominal aortae and aortic sinus cross-sections, we demonstrate that *Fap* deficiency decreased plaque formation in two atherosclerotic mouse models (-46% in *Apoe* and -34 % in *Ldlr* knockout mice). As a surrogate of plaque vulnerability fibrous cap thickness was used; it was increased in *Fap*-deficient mice, whereas Sirius red staining demonstrated that total collagen content remained unchanged. Using polarized light, atherosclerotic lesions from *Fap*-deficient mice displayed increased FAP targets in terms of enhanced collagen birefringence in plaques and increased pre-COL3A1 expression in aortic lysates. Analyses of the Stockholm Atherosclerosis Gene Expression (STAGE) data revealed that *FAP* expression was increased in human atherosclerotic compared to non-atherosclerotic arteries.

Conclusions. Our data provide causal evidence that constitutive *Fap* deletion decreases progression of experimental atherosclerosis and increases features of plaque stability with decreased collagen breakdown. Thus, inhibition of FAP expression or activity may not only represent a promising therapeutic target in atherosclerosis but appears safe at the experimental level for FAP-targeted cancer therapies.

Translational Perspective

Fibroblast activation protein (FAP) is upregulated at sites of chronic tissue remodelling including rheumatoid arthritis and solid tumours. Indeed, depletion of FAP-positive cells inhibits tumour growth by increasing antitumour immunity. FAP has also been correlated with human coronary plaques, whereby its causal role remains unknown. Our data provide causal evidence that constitutive *Fap* deletion decreases progression of experimental atherosclerosis and increases features of plaque stability. Thus, inhibition of FAP expression or activity may not only represent a novel therapeutic target for atherosclerosis but appears safe – at the experimental level – for FAP-targeted cancer therapies.

1. Introduction

Vulnerable plaques pose a central problem in human atherosclerosis. Their rupture may cause complete thrombotic arterial lumen obstruction, which may lead to myocardial infarction or stroke. A sufficiently thick fibrous cap ensures plaque stability and a barrier between blood and the prothrombotic necrotic core within the plaque [1, 2]. Collagenases (e.g. matrix metalloproteinases (MMPs) and cathepsins) degrade collagen within the fibrous cap, thereby thinning the cap and making them more prone to rupture [3]. Therefore, extra-cellular matrix-degrading collagenases have emerged as promising therapeutic targets against rupture of vulnerable plaque [4]. Interestingly, many collagenases involved in tissue remodelling such as rheumatoid arthritis or tumour expansion play similar roles in atherogenesis [3, 5].

Fibroblast activation protein (FAP) can be membrane-bound or soluble, and is a constitutively active serine protease that exhibits dipeptidyl peptidase IV activity and prolyl endopeptidase activity with a specificity for collagens [6-8]. Matrix turnover is a central event in the pathogenesis of chronic inflammatory diseases such as rheumatoid arthritis, tumour formation and atherosclerosis. Along these lines, FAP is expressed by activated fibroblasts in epithelial tumour stroma, arthritis and wound healing, but remains virtually undetectable in healthy tissues [6, 9-11]. In rheumatoid arthritis, FAP is expressed in SMA-positive myofibroblasts and associated with matrix metalloproteinase expression [9]. Moreover, a recent study showed that FAP was increased in cardiac fibrosis, which in turn promotes the development of various cardiac diseases and heart failure [12]. Interestingly, engineered chimeric (FAP-)antigen receptor (CAR) T cells could be used to target FAP in cardiac fibrosis; this strategy restored cardiac function in a hypertensive heart failure model [12].

Previously, we have reported that FAP expression is enhanced in human fibroatheromata versus plaque-free aortae, and its expression increases upon plaque progression [13]. Although expression of FAP protein correlated with the macrophage burden in human aortic plaques, colocalization images revealed that FAP was mainly expressed by smooth muscle cells [13].

Many collagenases involved in chronic tissue remodelling processes such as rheumatoid arthritis and tumour progression play similar roles in atherogenesis [3, 5]. Yet, the causal role of FAP in atherogenesis remains unknown. Therefore, we assessed the cause-effect relationship between the loss-of-function

of FAP and the phenotype of atherosclerosis by crossbreeding *Fap* knockout mice [14] with atherosclerosis-prone *apolipoprotein E* (*Apoe*) or *low-density lipoprotein receptor* (*Ldlr*) knockout mice.

2. Methods

2.1 Mice. Mice with a germline *Fap* deletion were obtained from the Centenary Institute, Sydney, AU [14, 15] and licensed from Boehringer Ingelheim Pharma GmbH & Co KG. Congenic C57BL6/J $Fap^{-/-}$ and $Fap^{+/+}$ mice were kept in a temperature-controlled facility with a 12-h light/dark cycle and free access to normal chow and water. To assess atherosclerosis development, $Fap^{-/-}$ mice were crossbred to either $Apoe^{-/-}$ or $Ldlr^{-/-}$ mice. Of those, male mice were fed a high-cholesterol diet (1.25% total cholesterol, Research Diets) for 12 weeks starting at the age of 8 weeks. After being anesthetised with isoflurane using a gas flow vaporizer (4.5 to 5% isoflurane) for 5 minutes, mice were euthanised by cardiac puncture and exsanguination.

2.2 Study approval. All animal experiments were approved by the Veterinary Office of the Canton Zurich (animal licenses: 189/2011 and 5263) and all procedures were in accordance to the guidelines from Directive 2010/63/EU of the European Parliament on the protection of animals used for scientific purposes.

2.3 FAP activity assay. The FAP specific enzyme assay was adapted from published assays [11, 16], using 100 uM Z-Gly-Pro-aminomethylcoumarin (AMC) as substrate, and the prolyl endopeptidase selective inhibitor S-17092 (Sigma-Aldrich #SML0181) at 0.1 uM to ensure FAP specificity.

2.4 FAP proteomics. Generation of *Fap*-deficient mouse embryonic fibroblasts and cultivation of the cells was described previously [8]. Terminal amine isotopic labelling of substrates (TAILS) and tests of data significance were performed previously [8].The statistically significant cleavages in collagens were arranged by location in primary structure and the cleavage sites that follow each Gly-Pro, the motif typical of FAP mediated cleavage, were identified.

2.5 Western blot analysis. 30 mg aortic lysates were pulverized using a steel tissue grinder, and then extracted in lysis buffer (50 mM Tris HCl pH 8.0, 125 mM NaCl, 0.25% NP-40, 0.5 mM phenylmethylsulfonyl fluoride, and protease/phosphatase inhibitor cocktail) for 10 minutes. The supernatant was transferred, and the protein content measured using Bradford reagent. Before running SDS-PAGE, protein lysates were boiled for 5 min at 95°C. Following proteins were used for Western blotting: anti-COL3A1 (22734-1-AP, Proteintech), anti-COL2A1 (sc-52658, Santa Cruz), anti-COL1A1 (PA1-26204, Invitrogen), anti-α tubulin (sc-8035, Santa Cruz), anti-βactin (sc-47778, Santa Cruz), and anti-GAPDH (TA802519, Origene).

2.6 Plasma lipid analysis. Total cholesterol (TC) and triglyceride (TG) plasma concentrations were measured using an enzymatic colorimetric assay (Biomerieux). To obtain lipoprotein fractions for fast-protein liquid chromatography (FPLC) analysis, each individual plasma sample was loaded on a filtration chromatography column onto a Superose 6 10/300 GL column (GE Healthcare), which allows separation of the three major lipoprotein classes (VLDLs, LDLs, HDLs and free glycerol) according to their size. Cholesterol and triglyceride concentrations were continuously measured in the effluent using an enzymatic colorimetric assay (Biomerieux) and results are expressed as O.D.

2.7 Immunohistochemistry. The heart-aortic root samples were stored in optimal cutting temperature (OCT) compound at -80°C, and then cut with a cryostat set at -20°C. The samples were then cut from the left ventricular basis towards the aortic valves. Once reaching the cusps, the specimen was re-orientated to achieve stringent cross-sectional cutting. 5 μm thick serial cross sections were then collected at approximately 100 μm intervals on microscopic glass slides until the aortic cusps were no longer visible. These 5 μm-thick serial cryosections were stained with Oil-red O (ORO), rat anti-CD68 (MCA 1957GA, Serotec), rat anti-CD3 (MCA 500GA, Serotec), rat anti-VCAM-1 (MCA 1129, Serotec), and rabbit anti-αSMA (D4K9N, Cell Signaling). Means were taken from at least 6 different mice evaluating at least 6 serial cryosections/tissue from each mouse. Thoraco-abdominal aortae were fixed with 4% paraformaldehyde and plaques stained with Oil-red O. Collagen content, fibrous cap thickness, and necrotic core size were analysed by Elastica van Gieson staining. Sirius Red stainings were performed to visualize collagen content under normal light.

2.8 Second harmonics. 5-μm-thick serial cryosections from the aortic sinus were used to perform second-harmonic generation of collagen fibers using two-photon microscopy. Second-harmonic signal was generated by tuning the Mai Tai Ti:sapphire laser to 880 nm and collecting the resultant tissue emission at 440 nm.

2.9 Gene expression analysis. Aortic RNAs were extracted using TRIZOL (Thermo Fisher, no. 15596026). For RT-qPCR, cDNA was generated using the All-in-One cDNA Synthesis kit (Biotool, no. B24403), and analysed by qPCR using a SYBR Green qPCR Master Mix (Biotool, no. B21202) and the primers listed in the online supplement (**Supplemental Table S4**). Expression data were normalized to housekeeping genes, i.e. *Actb*, *B2m and/or Ppib* mRNA levels.

2.10 Transcriptomic data analyses. The raw and/or normalized transcriptomic data from previous studies are publicly available on Gene Expression Omnibus (GEO; www.ncbi.nlm.nih.gov/geo) under the accession number GSE40231 (STAGE[17]) and analysed as described previously[18]. The *tabula muris* data can be accessed and analysed online (https://tabula-muris.ds.czbiohub.org). The single cell-RNA seq data was obtained from Prof. Qinbo Xu from the King's College London British Heart Foundation Centre (United Kingdom).[19]

2.11 Statistics. Data are presented as scatter plots plus mean. Comparison of differences between two groups was assessed using unpaired two-tailed Student's *t*-tests. A nonparametric Mann-Whitney test was used for the analysis of the SGH data since the data distribution did not pass the D'Agostino & Pearson omnibus normality test. Multiple group comparisons were assessed by ANOVA analysis and Bonferroni post-hoc tests, and multiplicity adjusted P values are displayed for the comparisons. Differences of $p < 0.05$ were considered statistically significant. Statistical analyses were performed using GraphPad Prism 6.

3. Results

3.1 Deletion of *Fap* protects against atherosclerosis

To address the causal role of endogenous FAP in atherogenesis, we crossbred *Fap*-deficient mice [15] with two different atherosclerosis-prone mouse models, i.e. *Ldlr*$^{-/-}$ and *Apoe*$^{-/-}$ mice [20] (**Supplemental Figure 1**). Deletion of FAP was assessed by genotyping and confirmed by measuring its enzymatic activity: FAP activity was abolished in both mouse models with constitutive *Fap* deletion (**Figure 1A, B**). We next placed 8-week old male mice on a high-cholesterol diet for 12 weeks and assessed atherosclerotic plaque development. Deletion of *Fap* diminished formation of atherosclerotic lesions by approximately one third in *Ldlr*$^{-/-}$ *Fap*$^{-/-}$ and by about half in *Apoe*$^{-/-}$ *Fap*$^{-/-}$ mice (**Figure 1C, D**). While *Apoe*$^{-/-}$ *Fap*$^{-/-}$ were slightly heavier than control *Apoe*$^{-/-}$ *Fap*$^{+/+}$ mice, no difference in body weight was noted in the *Ldlr*$^{-/-}$ background (**Supplemental Figure 2**).

We next examined whether plasma levels of total cholesterol and triglycerides at the time of harvesting correlated with the atherosclerosis phenotype. Total cholesterol content did not differ in any of the two atherosclerotic mouse models, while plasma triglyceride levels were increased in *Apoe*$^{-/-}$ *Fap*$^{-/-}$ but not in *Ldlr*$^{-/-}$ *Fap*$^{-/-}$ mice (**Supplemental Figure 3**). Hematological analyses did not reveal differences in the number of leukocytes subpopulations, erythrocytes or platelets between *Ldlr*$^{-/-}$ *Fap*$^{-/-}$ and *Ldlr*$^{-/-}$ *Fap*$^{+/+}$ mice (**Supplemental Table 1**). On the other side, *Apoe*$^{-/-}$ *Fap*$^{-/-}$ had a reduced amount of blood neutrophils and platelets, and an increased number of monocytes compared to *Apoe*$^{-/-}$ *Fap*$^{+/+}$ controls. *Apoe* knockout mice on a high-cholesterol diet display a stronger pro-inflammatory and atherogenic phenotype compared with *Ldlr*$^{-/-}$ mice [20], which could be related to the differences observed in leukocyte subpopulations (**Supplemental Table 1**).

3.2 *Fap*-deletion increases protective fibrous cap thickness

To better characterize the atherosclerotic lesions, we carried out several immunohistochemical stainings on cross-sections of the aortic sinus of *Apoe*$^{-/-}$ *Fap*$^{-/-}$ and *Apoe*$^{-/-}$ *Fap*$^{+/+}$ mice. Along with the reduced number of thoraco-abdominal lesions, *Apoe*$^{-/-}$ *Fap*$^{-/-}$ mice displayed reduced content of neutral lipids in the aortic sinus compared to *Apoe*$^{-/-}$ *Fap*$^{+/+}$ mice (**Figure 2A and Supplemental Figure 4**). Interestingly, we did not observe any difference in the amount of the vascular cell adhesion molecule 1 (VCAM-1), macrophages (CD68^{+} cells), or T cells (CD3^{+} cells) between the two genotypes (**Figure 2B**

– D). These findings suggest that the atherosclerotic phenotype is not secondary to a differential accumulation of immune cells within the lesions.

Since FAP is an extra-cellular matrix-degrading collagenase, we performed Elastica van Gieson stainings to measure the content of collagen and to assess advanced plaque parameters in aortic sinus cross-sections. Surprisingly, there was no significant difference in the content of collagen in *Apoe*$^{-/-}$ *Fap*$^{-/-}$ compared to *Apoe*$^{-/-}$ *Fap*$^{+/+}$ mice (**Figure 3A**). However, atherosclerotic lesions from *Apoe*$^{-/-}$ *Fap*$^{-/-}$ mice displayed larger fibrous caps, whereas the size of the necrotic cores was comparable to *Apoe*$^{-/-}$ *Fap*$^{+/+}$ mice (**Figure 3B-D**), suggesting that *Apoe*$^{-/-}$ *Fap*$^{-/-}$ mice do not only develop less atherosclerosis, but their lesions are also less prone to rupture. α-smooth mucle actin (α-SMA) staining showed a trend for increased vascular smooth mucle cell content within the atherosclerotic lesions, suggesting that vascular smooth cells migrated into the plaques to reinforce the fibrous cap (**Supplemental Figure 5**).

3.3 Altered collagen organization in aortic sinus lesions from *Fap*-deficient mice

We next performed Sirius red stainings as a alternative method to quantify the collagen content. It confirmed that there is no difference in collagen content between the genotypes (**Figure 3E**). Previously, Santos et al. showed that tumours from *Fap*-deficient mice (with a LacZ knockin, *Fap*$^{lacZ/lacZ}$) display increased collagen birefringence under polarised light in comparison to wildtype mice [21], suggesting a reduced organization of the collagen fibers. To investigate a possible change in collagen organization, we performed second-harmonic generation (SHG) of collagen on aortic sinus lesions using two-photon microscopy laser microscopy [22, 23]. These analyses revealed that lesions of *Apoe*$^{-/-}$ *Fap*$^{-/-}$ mice displayed increased SHG signals compared to *Apoe*$^{-/-}$ *Fap*$^{+/+}$ mice (**Figure 3F**), confirming that deletion of FAP indeed augments the deposition of fibrillar collagens in these lesions.

3.4 Proteomic analysis demonstrates that FAP cleaves several collagens

To investigate the underlying mechanisms, we first analysed the expression of collagens, extracellular matrix proteases and fibrosis markers in the aortae. Despite a trend for increases fibrosis markers, we observed no significant difference of the transcripts at mRNA level (**Supplemental Figure 6**). In order to understand how FAP induces the observed changes in collagen structure, we drilled down into our targeted proteomic analyses of cell culture supernatants from *Fap*$^{-/-}$ mouse embryonic fibroblasts to identify potential collagen targets of FAP. We had found by stable isotope labelling with amino acids in cell culture (SILAC) that the quantities of collagens 3, 5 and 6 differed in the presence of enzymatically

active FAP compared to inactive FAP [8]. In addition, terminal amine isotopic labelling of substrates (TAILS) showed that the major collagen species COL1A1, COL1A2, COL5A2 and COL3A1 are proteolytic targets of FAP in murine fibroblast cultures. The multiple cleavage sites in these precollagens are probably generated co-operatively by FAP with other collagenases [8]. However, we found that many of these cleavage sites followed Gly-Pro, which is prototypical of FAP-induced hydrolysis, and that most of the greatest increases in collagen fragmentation were coincident with cleavage after Gly-Pro (**Figure 4A-D**).

3.5 Reduced cleavage of pre-COL3A1 in *Fap* knockout mice

To validate the SILAC-TAILS data and verify if collagen degradation could also be affected in the Fap-deficient mice, we analysed the protein expression of the three main collagens in aortic lysates of *Apoe*$^{-/-}$ *Fap*$^{-/-}$ and *Apoe*$^{-/-}$ *Fap*$^{+/+}$ mice. Interestingly, we observed an increase of the precursor of COL3A1 in *Apoe*$^{-/-}$ *Fap*$^{-/-}$ compared to *Apoe*$^{-/-}$ *Fap*$^{+/+}$ aortae (**Figure 4E, F, and Supplemental Figure 7A**), suggesting that the precursor cannot be properly cleaved in FAP-deficient mice. Conversely, COL1A1 and COL2A1 products were not altered between the two genotypes (**Supplemental Figure 7C-F**). Noteworthy, there is no known molecular basis for this preference of FAP for COL3 over other collagen subtypes.

3.6 Pathway analyses of FAP-expressing cells supports its role in collagen remodelling

Previously studies showed that FAP is mainly expressed in fibroblast and vascular smooth muscle cells. Analysis of the transcriptome of targeted aortic fluorescent activated cell sorting (FACS)-isolated aortic cell available at *Tabula muris* [24] showed and confirmed that FAP is mainly expressed by fibroblasts (**Supplemental Figure 8**). Since these were aortae from non-atherosclerotic mice, we further analysed an untargeted single cell RNA-sequencing dataset from aortae of *Apoe* knockout mice [19]. We first selected all cells displaying *FAP* sequencing counts (>2), and then filtered the top 20 highest expressed transcripts of each of these cells (**Supplemental Table S2**). Interestingly, pathway analysis shows enrichment of extracellular remodelling, such as collagen and extracellular fibril organisation, extracellular matrix and exosome, and collagen binding (**Supplemental Table S3**).

3.7 Increased expression of *FAP* in human atherosclerotic vessels

To evaluate whether the expression of FAP could be altered in human atherosclerotic plaques compared to healthy arteries, we compared the expression of *FAP* in atherosclerotic aortic roots to non-atherosclerotic mammary arteries from the Stockholm Atherosclerosis Gene Expression (STAGE)[17] study. Atherosclerotic aortae revealed an increased expression of *FAP* as compared to non-atherosclerotic mammary arteries (**Figure 4G**). Together, these data suggest that *FAP* expression is increased in human atherosclerotic plaques and could be a promising target for pharmacologic inhibition.

4. Discussion

In a previous study, we demonstrated that FAP expression is increased in human fibroatheromata versus plaque-free aortae, and that its expression positively correlates with the stages of plaque progression [13]. Moreover, soluble FAP cleaves α2-antiplasmin, which enhances its activity and incorporation into fibrin clots, thus promoting coagulation [25]. Surprisingly, the levels of circulating FAP are reduced in patients with coronary artery disease or stroke [26-29], and suggest that tissue resident and circulating FAP are independent markers of cardiovascular diseases [30].

The current study provides the following novel findings (**Figure 5**):

1) Constitutive genetic *Fap* loss-of-function in atherosclerosis-prone *Apoe* or *Ldlr*-deficient mice decreases plaque formation that is independent of plasma lipid levels. Moreover, the content of plaque VCAM-1, macrophages, and T cells was not different between the groups.

2) *Fap* deletion increases features of plaque stability with increased fibrous cap thickness. Analyses of aortic roots demonstrated that atherosclerotic lesions from *Apoe*$^{-/-}$ *Fap*$^{-/-}$ mice harbour thicker fibrous caps.

3) Plaque matrix analyses display increased SHG signals compared to *Apoe*$^{-/-}$ *Fap*$^{+/+}$ mice. The enhanced SHG signal suggests that the deletion of *Fap* increases deposition of fibrillar collagens in the lesions.

Using a targeted proteomic analyses of cell culture supernatants from *Fap*$^{-/-}$ mouse embryonic fibroblasts that express enzymatically active FAP or inactive FAP, we showed that FAP cleaves major collagens species at several sites, including COL3A1. When analysing COL3A1 protein expression in aortic lysates, we detected reduced cleavage of pre-COL3A1 in *Apoe*$^{-/-}$ *Fap*$^{-/-}$ compared to *Apoe*$^{-/-}$ *Fap*$^{+/+}$ mice. Notably, in a recent study with acromegaly patients, surgical or medical treatment of the pituitary somatotroph tumour markedly reduced the levels of FAP compared to untreated subjects. These effects were closely associated with a reduction in biomarkers of collagen turnover [31].

The exact mechanisms by which impaired COL3A1 expression and/or processing affect collagen fibril organization is not yet well known. In the first *Col3a1* knockout study, Rudolph Jaenisch's group demonstrated that collagen SHG imaging of fibroblast-derived matrices showed that *Col3*-deficient fibroblasts produced a more aligned and fibrillar matrix than wild-type cells, and that COL3A1 is crucial

for collagen I fibrillogenesis [32]. Therefore, changes in COL3A1 processing have an impact on the formation of fibrillar collagens.

Moreover, the vascular (type IV) form of the Ehlers-Danlos Syndrome, which is caused by mutations in the *COL3A1* gene, leads to an impaired fibrillar collagen disposition [32-36]. Both exon-skipping or missense mutations in the *COL3A1* loci can disrupt the collagen triple helix. These malformed helixes are then degraded or accumulate in intracellular compartments, and hence not secreted into the extracellular matrix. As a consequence, the reduction in COL3A1 caused by the mutations alters the size and structure of collagen fibrils [34]. Nevertheless, the precise mechanisms by which mutant COL3A1 causes dermal and vascular fragility remain largely unexplored.

Taken together, our current mouse and published human data [13] demonstrate that endogenous pro-oncogenic FAP promotes atherosclerosis development. Interestingly, depletion of FAP-positive cells inhibits tumour growth by increasing antitumour immunity [21], and small antagonists and blocking antibodies for FAP are already being applied in oncology [37]. Along these lines, it will not only be exciting to further test the impact of FAP inhibition on atherosclerosis in the experimental and clinical setting, FAP targeting may also comprise a promising cardio-oncological treatment avenue.

Interestingly, a recent study suggest that FAP also plays a central role in cardiac fibrosis, which promotes the development of various cardiac diseases and heart failure [12]. The authors showed that engineered chimeric FAP-antigen receptor T cells can be used to reduce experimental cardiac fibrosis and restore cardiac function using an angiotensin II/phenylephrine-induced hypertensive heart failure mouse model [12].

Thus, FAP appears an attractive therapeutic target for fibrotic heart failure and atherosclerosis worth being further investigated in the clinical arena.

Funding

This work was supported by the Swiss National Science Foundation (PZOOP3_161521 to S.S. and 310030_165990 and 320030_189229 to C.M.M.), the Novartis Foundation for medical-biological Research (#16B103 to S.S.), the Olga-Mayenfisch Foundation (to S.S.), the SwissLife Foundation (to S.S.), and the OPO Foundation (to S.S.), the Swiss Heart Foundation (to S.N.-S., S.S. and C.M.M.), and by Matching Funds UZH, University Research Priority Program Integrative Human Physiology at the University of Zurich (to C.M.M.).

Conflict of Interest

None declared.

Author Contributions

- Christian Matter initiated the study.
- Sokrates Stein and Christian Matter designed the experiments and co-supervised the study.
- Julien Weber, Stefanie Nusser-Stein, Jürgen Pahla, Shafeeq Mohammed, Sara Oppi, Daniel S. Gaul, and Sokrates Stein performed experiments and data analyses.
- Hui E. Zhang and Mark D. Gorrell performed the SILAC-mass spec analysis.
- Ferdinand von Meyenn provided support with the scRNA-seq analyses.
- Anne Tailleux and Bart Staels performed lipoprotein analyses.
- Sokrates Stein, Christian Matter, and Mark D. Gorrell wrote the manuscript.
- Francesco Paneni, Frank Ruschitzka and Thomas F. Lüscher edited the manuscript.
- Christian Matter, Sokrates Stein, Frank Ruschitzka and Thomas F. Lüscher obtained funding for the study.

Data Availability Statement

The data underlying this article is either publicly available (transcriptomic data) or will be shared on reasonable request to the corresponding author.

References

1. Stary HC, Chandler AB, Dinsmore RE, Fuster V, Glagov S, Insull Jr W, Rosenfeld ME, Schwartz CJ, Wagner WD, Wissler RW. A Definition of Advanced Types of Atherosclerotic Lesions and a Histological Classification of Atherosclerosis. *Arterioscler Thromb Vasc Biol* 1995:1512-1531.

2. Stary HC, Chandler AB, Glagov S, Guyton JR, Insull Jr W, Rosenfeld ME, Schaffer SA, Schwartz CJ, Wagner WD, Wissler RW. A definition of initial, fatty streak, and intermediate lesions of atherosclerosis. A report from the Committee on Vascular Lesions of the Council on Arteriosclerosis, American Heart Association. *Arterioscler Thromb Vasc Biol* 1994;**1994**:840-856.

3. Galis ZS, Sukhova GK, Lark MW, Libby P. Increased Expression of Matrix Metalloproteinases and Matrix Degrading Activity in Vulnerable Regions of Human Atherosclerotic Plaques. *J Clin Invest* 1994;**94**:2493-2503.

4. Libby P. Mechanisms of acute coronary syndromes and their implications for therapy. *The New England journal of medicine* 2013;**368**:2004-2013.

5. Libby P, Kobold S. Inflammation: a common contributor to cancer, aging, and cardiovascular diseases-expanding the concept of cardio-oncology. *Cardiovasc Res* 2019;**115**:824-829.

6. Park JE, Lenter MC, Zimmermann RN, Garin-Chesa P, Old LJ, Rettig WJ. Fibroblast activation protein, a dual specificity serine protease expressed in reactive human tumor stromal fibroblasts. *J Biol Chem* 1999;**274**:36505-36512.

7. Christiansen VJ, Jackson KW, Lee KN, McKee PA. Effect of fibroblast activation protein and alpha2-antiplasmin cleaving enzyme on collagen types I, III, and IV. *Arch Biochem Biophys* 2007;**457**:177-186.

8. Zhang HE, Hamson EJ, Koczorowska MM, Tholen S, Chowdhury S, Bailey CG, Lay AJ, Twigg SM, Lee Q, Roediger B, Biniossek ML, O'Rourke MB, McCaughan GW, Keane FM, Schilling O, Gorrell MD. Identification of Novel Natural Substrates of Fibroblast Activation Protein-alpha by Differential Degradomics and Proteomics. *Molecular & cellular proteomics : MCP* 2019;**18**:65-85.

9. Bauer S, Jendro MC, Wadle A, Kleber S, Stenner F, Dinser R, Reich A, Faccin E, Godde S, Dinges H, Muller-Ladner U, Renner C. Fibroblast activation protein is expressed by rheumatoid myofibroblast-like synoviocytes. *Arthritis Res Ther* 2006;**8**:R171.

10. Edosada CY, Quan C, Wiesmann C, Tran T, Sutherlin D, Reynolds M, Elliott JM, Raab H, Fairbrother W, Wolf BB. Selective inhibition of fibroblast activation protein protease based on dipeptide substrate specificity. *J Biol Chem* 2006;**281**:7437-7444.

11. Keane FM, Yao TW, Seelk S, Gall MG, Chowdhury S, Poplawski SE, Lai JH, Li Y, Wu W, Farrell P, Vieira de Ribeiro AJ, Osborne B, Yu DM, Seth D, Rahman K, Haber P, Topaloglu AK, Wang C, Thomson S, Hennessy A, Prins J, Twigg SM, McLennan SV, McCaughan GW, Bachovchin WW, Gorrell MD. Quantitation of fibroblast activation protein (FAP)-specific protease activity in mouse, baboon and human fluids and organs. *FEBS Open Bio* 2013;**4**:43-54.

12. Aghajanian H, Kimura T, Rurik JG, Hancock AS, Leibowitz MS, Li L, Scholler J, Monslow J, Lo A, Han W, Wang T, Bedi K, Morley MP, Linares Saldana RA, Bolar NA, McDaid K, Assenmacher CA, Smith CL, Wirth D, June CH, Margulies KB, Jain R, Pure E, Albelda SM, Epstein JA. Targeting cardiac fibrosis with engineered T cells. *Nature* 2019;**573**:430-433.

13. Brokopp CE, Schoenauer R, Richards P, Bauer S, Lohmann C, Emmert MY, Weber B, Winnik S, Aikawa E, Graves K, Genoni M, Vogt P, Luscher TF, Renner C, Hoerstrup SP, Matter CM. Fibroblast activation protein is induced by inflammation and degrades type I collagen in thin-cap fibroatheromata. *Eur Heart J* 2011;**32**:2713-2722

14. Tan SY, Chowdhury S, Polak N, Gorrell MD, Weninger W. Fibroblast activation protein is dispensable in the anti-influenza immune response in mice. *PLoS One* 2017;**12**:e0171194.

15. Niedermeyer J, Kriz M, Hilberg F, Garin-Chesa P, Bamberger U, Lenter MC, Park J, Viertel B, Puschner H, Mauz M, Rettig WJ, Schnapp A. Targeted disruption of mouse fibroblast activation protein. *Mol Cell Biol* 2000;**20**:1089-1094.

16. Lee KN, Jackson KW, Christiansen VJ, Lee CS, Chun JG, McKee PA. Antiplasmin-cleaving enzyme is a soluble form of fibroblast activation protein. *Blood* 2006;**107**:1397-1404.

17. Hagg S, Skogsberg J, Lundstrom J, Noori P, Nilsson R, Zhong H, Maleki S, Shang MM, Brinne B, Bradshaw M, Bajic VB, Samnegard A, Silveira A, Kaplan LM, Gigante B, Leander K, de Faire U, Rosfors S, Lockowandt U, Liska J, Konrad P, Takolander R, Franco-Cereceda A, Schadt EE, Ivert T, Hamsten A, Tegner J, Bjorkegren J. Multi-organ expression profiling uncovers a gene module in coronary artery disease involving transendothelial migration of leukocytes and LIM domain binding 2: the Stockholm Atherosclerosis Gene Expression (STAGE) study. *PLoS Genet* 2009;**5**:e1000754.

18. Oppi S, Nusser-Stein S, Blyszczuk P, Wang X, Jomard A, Marzolla V, Yang K, Velagapudi S, Ward LJ, Yuan XM, Geiger MA, Guillaumon AT, Othman A, Hornemann T, Rancic Z, Ryu D, Oosterveer MH, Osto E, Luscher TF, Stein S. Macrophage NCOR1 protects from atherosclerosis by repressing a pro-atherogenic PPARgamma signature. *Eur Heart J* 2020;**41**:995-1005.

19. Gu W, Ni Z, Tan YQ, Deng J, Zhang SJ, Lv ZC, Wang XJ, Chen T, Zhang Z, Hu Y, Jing ZC, Xu Q. Adventitial Cell Atlas of wt (Wild Type) and ApoE (Apolipoprotein E)-Deficient Mice Defined by Single-Cell RNA Sequencing. *Arterioscler Thromb Vasc Biol* 2019;**39**:1055-1071.

20. Oppi S, Luscher TF, Stein S. Mouse Models for Atherosclerosis Research-Which Is My Line? *Front Cardiovasc Med* 2019;**6**:46.

21. Santos AM, Jung J, Aziz N, Kissil JL, Pure E. Targeting fibroblast activation protein inhibits tumor stromagenesis and growth in mice. *J Clin Invest* 2009;**119**:3613-3625.

22. Hutcheson JD, Goettsch C, Bertazzo S, Maldonado N, Ruiz JL, Goh W, Yabusaki K, Faits T, Bouten C, Franck G, Quillard T, Libby P, Aikawa M, Weinbaum S, Aikawa E. Genesis and growth of extracellular-vesicle-derived microcalcification in atherosclerotic plaques. *Nat Mater* 2016;**15**:335-343.

23. Cox G, Kable E, Jones A, Fraser I, Manconi F, Gorrell MD. 3-dimensional imaging of collagen using second harmonic generation. *J Struct Biol* 2003;**141**:53-62.

24. Tabula Muris C, Overall c, Logistical c, Organ c, processing, Library p, sequencing, Computational data a, Cell type a, Writing g, Supplemental text writing g, Principal i. Single-cell transcriptomics of 20 mouse organs creates a Tabula Muris. *Nature* 2018;**562**:367-372.

25. Uitte de Willige S, Malfliet J, Abdul S, Leebeek FWG, Rijken DC. The level of circulating fibroblast activation protein correlates with incorporation of alpha-2-antiplasmin into the fibrin clot. *Thromb Res* 2018;**166**:19-21.

26. Uitte de Willige S, Malfliet JJ, Deckers JW, Dippel DW, Leebeek FW, Rijken DC. Plasma levels of soluble fibroblast activation protein in arterial thrombosis: determinants and cleavage of its substrate alpha-2-antiplasmin. *Int J Cardiol* 2015;**178**:105-110.

27. Tillmanns J, Widera C, Habbaba Y, Galuppo P, Kempf T, Wollert KC, Bauersachs J. Circulating concentrations of fibroblast activation protein alpha in apparently healthy individuals and patients with acute coronary syndrome as assessed by sandwich ELISA. *Int J Cardiol* 2013;**168**:3926-3931.

28. Tillmanns J, Fraccarollo D, Galuppo P, Wollert KC, Bauersachs J. Changes in concentrations of circulating fibroblast activation protein alpha are associated with myocardial damage in patients with acute ST-elevation MI. *Int J Cardiol* 2017;**232**:155-159.

29. Baerts L, Brouns R, Kehoe K, Verkerk R, Engelborghs S, De Deyn PP, Hendriks D, De Meester I. Acute Ischemic Stroke Severity, Progression, and Outcome Relate to Changes in Dipeptidyl Peptidase IV and Fibroblast Activation Protein Activity. *Transl Stroke Res* 2017;**8**:157-164.

30. Lay AJ, Zhang HE, McCaughan GW, Gorrell MD. Fibroblast activation protein in liver fibrosis. *Front Biosci (Landmark Ed)* 2019;**24**:1-17.

31. Arlien-Soborg MC, Grondahl C, Baek A, Dal J, Alle Madsen M, Hogild ML, Pedersen SB, Bjerre M, Jorgensen JOL. Fibroblast activation protein is a GH target: A prospective study of patients with acromegaly before and after treatment. *J Clin Endocrinol Metab* 2019.

32. Liu X, Wu H, Byrne M, Krane S, Jaenisch R. Type III collagen is crucial for collagen I fibrillogenesis and for normal cardiovascular development. *Proc Natl Acad Sci U S A* 1997;**94**:1852-1856.

33. D'Hondt S, Guillemyn B, Syx D, Symoens S, De Rycke R, Vanhoutte L, Toussaint W, Lambrecht BN, De Paepe A, Keene DR, Ishikawa Y, Bachinger HP, Janssens S, Bertrand MJM, Malfait F. Type III collagen affects dermal and vascular collagen fibrillogenesis and tissue integrity in a mutant Col3a1 transgenic mouse model. *Matrix Biol* 2018;**70**:72-83.

34. Mao JR, Bristow J. The Ehlers-Danlos syndrome: on beyond collagens. *J Clin Invest* 2001;**107**:1063-1069.

35. Schwarze U, Schievink WI, Petty E, Jaff MR, Babovic-Vuksanovic D, Cherry KJ, Pepin M, Byers PH. Haploinsufficiency for one COL3A1 allele of type III procollagen results in a

phenotype similar to the vascular form of Ehlers-Danlos syndrome, Ehlers-Danlos syndrome type IV. *Am J Hum Genet* 2001;**69**:989-1001.

36. Smith LB, Hadoke PW, Dyer E, Denvir MA, Brownstein D, Miller E, Nelson N, Wells S, Cheeseman M, Greenfield A. Haploinsufficiency of the murine Col3a1 locus causes aortic dissection: a novel model of the vascular type of Ehlers-Danlos syndrome. *Cardiovasc Res* 2011;**90**:182-190.

37. Busek P, Mateu R, Zubal M, Kotackova L, Sedo A. Targeting fibroblast activation protein in cancer - Prospects and caveats. *Front Biosci (Landmark Ed)* 2018;**23**:1933-1968.

Figures legends

Figure 1. *Constitutive Fap deletion reduces atherosclerosis development in mice*. (**A, B**) FAP activity assay performed with plasma obtained from indicated mouse lines. (**A**) FAP activity as assessed by the FAP target 3144-aminomethylcoumarin (AMC) release curve. (**B**) Quantification of the AMC release over time. n = 5 per genotype, n = 2 for controls. rhFAP, recombinant human FAP. (**C, D**) Quantification and representative images of atherosclerotic lesions in thoraco-abdominal aortae stained with Oil-red O in the indicated genotypes. n ≥ 16 per genotype. Scatter blots with means. (Adjusted) P values are indicated in the figures (99.9% confidence interval). Unpaired two-tailed Student's *t*-test (**C, D**); ANOVA analysis and Bonferroni post-hoc test (**B**).

Figure 2. *Fap* deficiency diminishes accumulation of neutral lipids in atherosclerotic plaques of *Apoe*$^{-/-}$ mice without affecting macrophages and T cells. (**A**) Quantification of neutral lipids and representative images of aortic sinus cross-sections with Oil-red O. (**B-D**) Quantification of immunohistochemical stainings and representative images of VCAM-1 (**B**), CD68 (**C**), and CD3 (**D**) in cross-sections from the aortic sinus. n ≥ 8 per genotype (4 cross-sections per mouse). Black bars = 400 μm, orange bars = 40 μm. Black arrows, examples of CD3-positive cells. Scatter blots with means, unpaired two-tailed Student's *t*-test.

Figure 3. ***Fap deletion alters collagen structure in atherosclerotic lesions*.** (**A-D**) Quantification of total collagen content (**A**), necrotic core size (**B**), fibrous cap thickness (**C**), and (**D**) representative images of aortic sinus cross-sections stained with Elastica van Gieson (EvG). Green line, fibrous cap; dashed green line, necrotic core. n = 7 *Apoe*$^{-/-}$ *Fap*$^{+/+}$ mice, n = 9 *Apoe*$^{-/-}$ *Fap*$^{-/-}$. (**E**) Quantification of collagen content and representative images of aortic sinus cross-sections stained with Sirius Red and visualized under normal light. n = 7 *Apoe*$^{-/-}$ *Fap*$^{+/+}$ mice, n = 9 *Apoe*$^{-/-}$ *Fap*$^{-/-}$. (**F**) Representative images of second harmonics generation (SHG) and quantification of fibrillar collagen in aortic sinus cross-sections. n = 9 *Apoe*$^{-/-}$ *Fap*$^{+/+}$ mice, n = 6 *Apoe*$^{-/-}$ *Fap*$^{-/-}$. Black and white bars = 400 μm, orange bars = 100 μm. Scatter blots with means, unpaired two-tailed Student's *t*-test (**A-E**); nonparametric Mann-Whitney test (**F**).

Figure 4. *Cleavage events in collagens revealed by proteomics in the secretomes of mouse embryonic fibroblasts that express active FAP compared with inactive FAP*. (**A-D**) Log transformed fold-change of neo-N-terminal peptides is shown for individual cleavage sites and arranged by amino acid position for COL1A1 (**A**), COL1A2 (**B**), COL3A1 (**C**), and COL5A2 (**D**). Neo-N-terminal peptides resulting from cleavage after Gly-Pro are represented by coloured squares, whereas other cleavage sites are plotted as black circles. A fold change ≥ 0.58 represents increased peptide abundance of ≥ 50% in the presence of FAP activity. A fold change ≤ -0.58 represents decreased peptide abundance of ≥ 50% in the presence of FAP activity. Mean and standard deviation of data that reached significance (limma statistic with $p < 0.05$). (**E, F**) COL3A1 immunoblots from aortae from *Apoe*$^{-/-}$ *Fap*$^{-/-}$ and *Apoe*$^{-/-}$ *Fap*$^{+/+}$ mice. Pre, precursor COL3A1; cleaved, cleaved COL3A1 fibers. n = 4 per genotype. (**G**) Expression of *FAP* in biopsies of non-atherosclerotic mammary arteries (Mammary) and atherosclerotic aortic roots (Athero) (raw data, GSE40231). Unpaired two-tailed Student's *t*-test (**F, G**).

Figure 5. Graphical abstract. Scheme demonstrating how the deletion of FAP protects against atherosclerosis development.

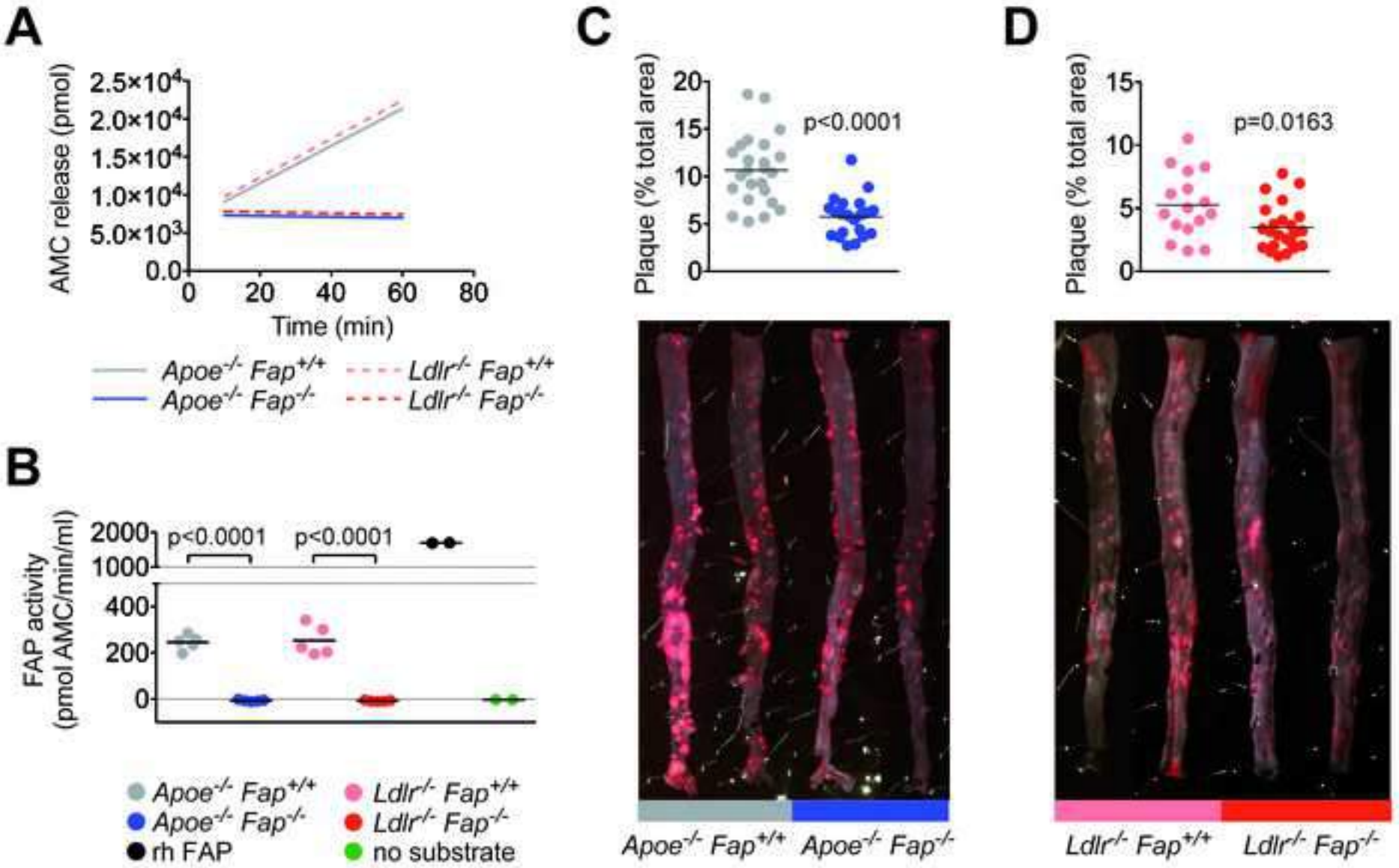
A
AMC release (pmol)
2.5×10^4
2.0×10^4
1.5×10^4
1.0×10^4
5.0×10^3
0.0
0
20
40
60
80
Time (min)
Apoe-/- Fap+/+
Apoe-/- Fap-/-
Ldlr-/- Fap+/+
Ldlr-/- Fap-/-
B
FAP activity (pmol AMC/min/ml)
2000
1000
400
200
0
p<0.0001
p<0.0001
Apoe-/- Fap+/+
Apoe-/- Fap-/-
rh FAP
Ldlr-/- Fap+/+
Ldlr-/- Fap-/-
no substrate
C
Plaque (% total area)
20
15
10
5
0
p<0.0001
Apoe-/- Fap+/+
Apoe-/- Fap-/-
D
Plaque (% total area)
15
10
5
0
p=0.0163
Ldlr-/- Fap+/+
Ldlr-/- Fap-/-

Figure 2

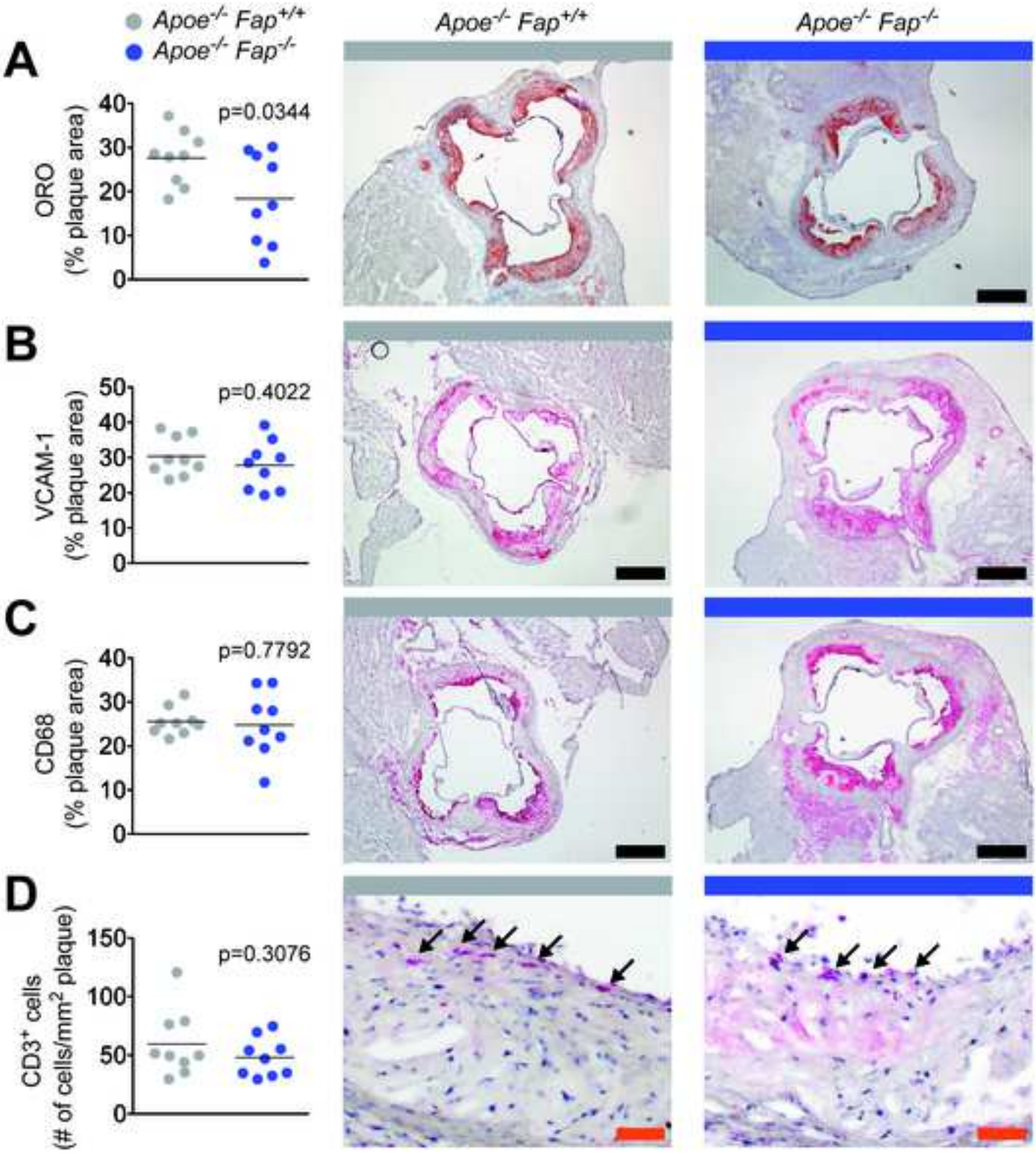
Apoe-/- Fap+/+
Apoe-/- Fap-/-
A
ORO
(% plaque area)
p=0.0344
B
VCAM-1
(% plaque area)
p=0.4022
C
CD68
(% plaque area)
p=0.7792
D
CD3+ cells
(# of cells/mm2 plaque)
p=0.3076

Figure 3

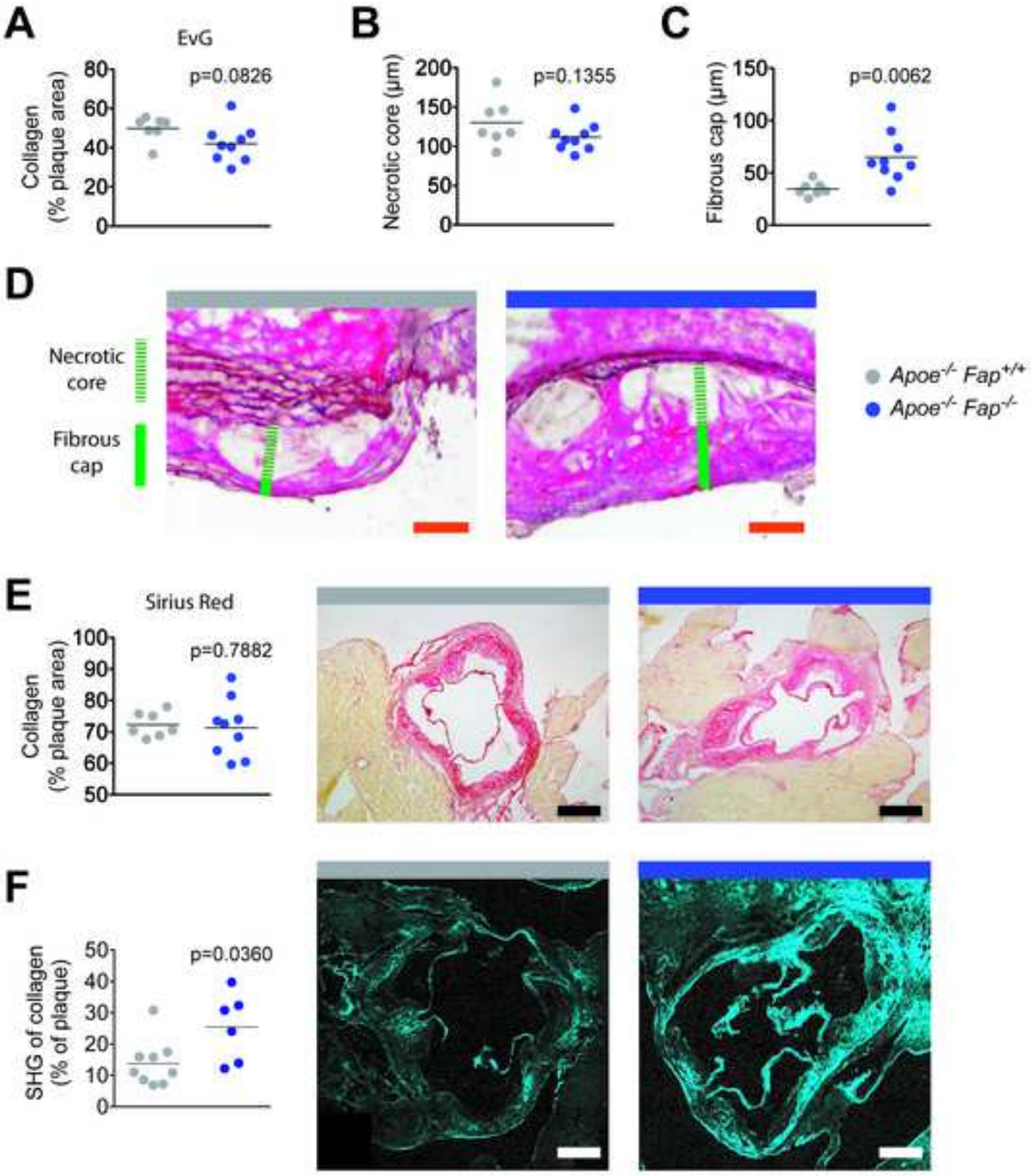
A
EvG
Collagen (% plaque area)
80
60
40
20
0
p=0.0826
B
Necrotic core (µm)
200
150
100
50
0
p=0.1355
C
Fibrous cap (µm)
150
100
50
0
p=0.0062
D
Necrotic core
Fibrous cap
Apoe-/- Fap+/+
Apoe-/- Fap-/-
E
Sirius Red
Collagen (% plaque area)
100
90
80
70
60
50
p=0.7882
F
SHG of collagen (% of plaque)
50
40
30
20
10
0
p=0.0360

Figure 4

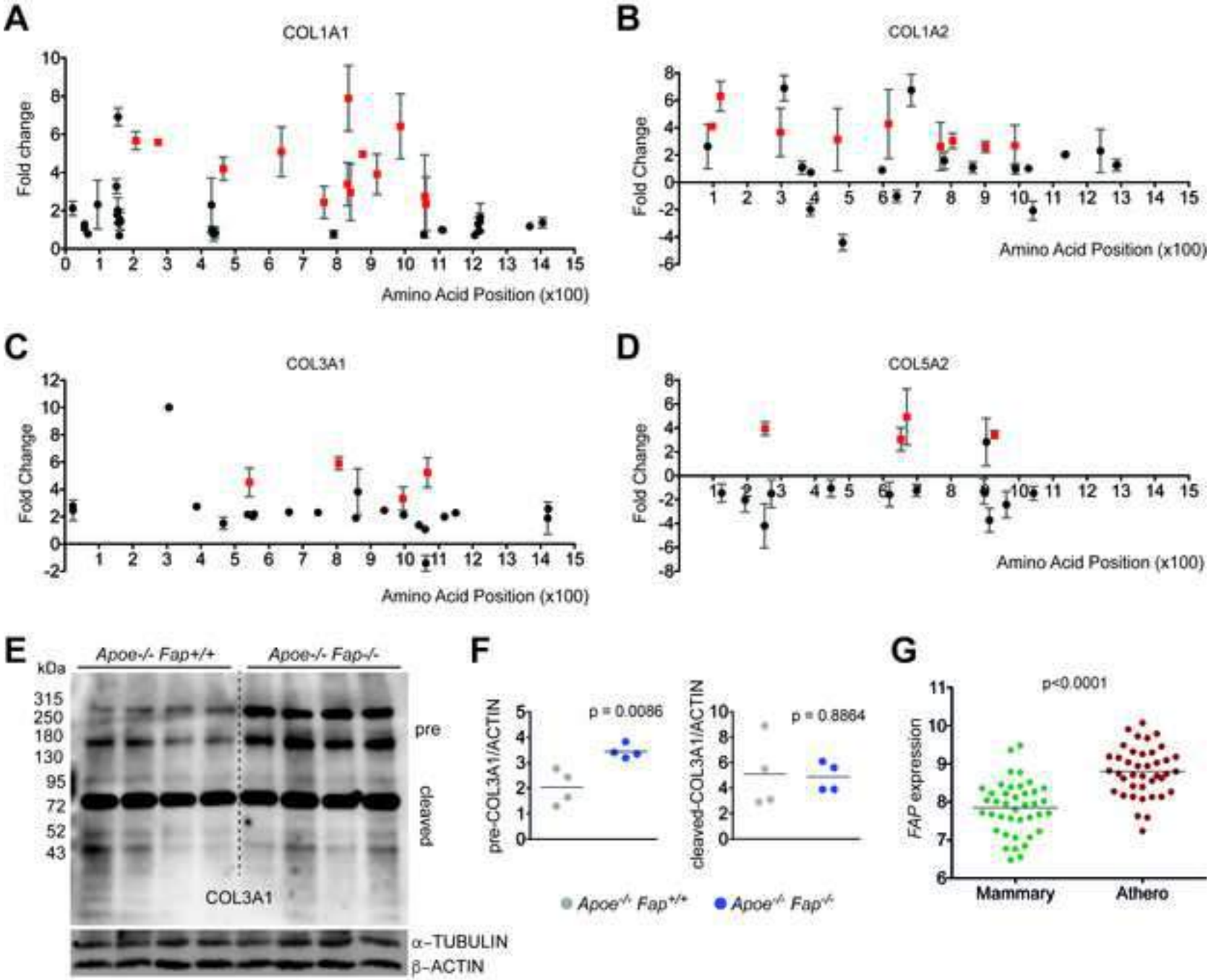
A
COL1A1
Fold change
Amino Acid Position (x100)
B
COL1A2
Fold Change
Amino Acid Position (x100)
C
COL3A1
Fold Change
Amino Acid Position (x100)
D
COL5A2
Fold Change
Amino Acid Position (x100)
E
Apoe-/- Fap+/+
Apoe-/- Fap-/-
kDa
315
250
180
130
95
72
52
43
pre
cleaved
COL3A1
α-TUBULIN
β-ACTIN
F
pre-COL3A1/ACTIN
p = 0.0086
cleaved-COL3A1/ACTIN
p = 0.8864
Apoe-/- Fap+/+
Apoe-/- Fap-/-
G
p<0.0001
FAP expression
Mammary
Athero

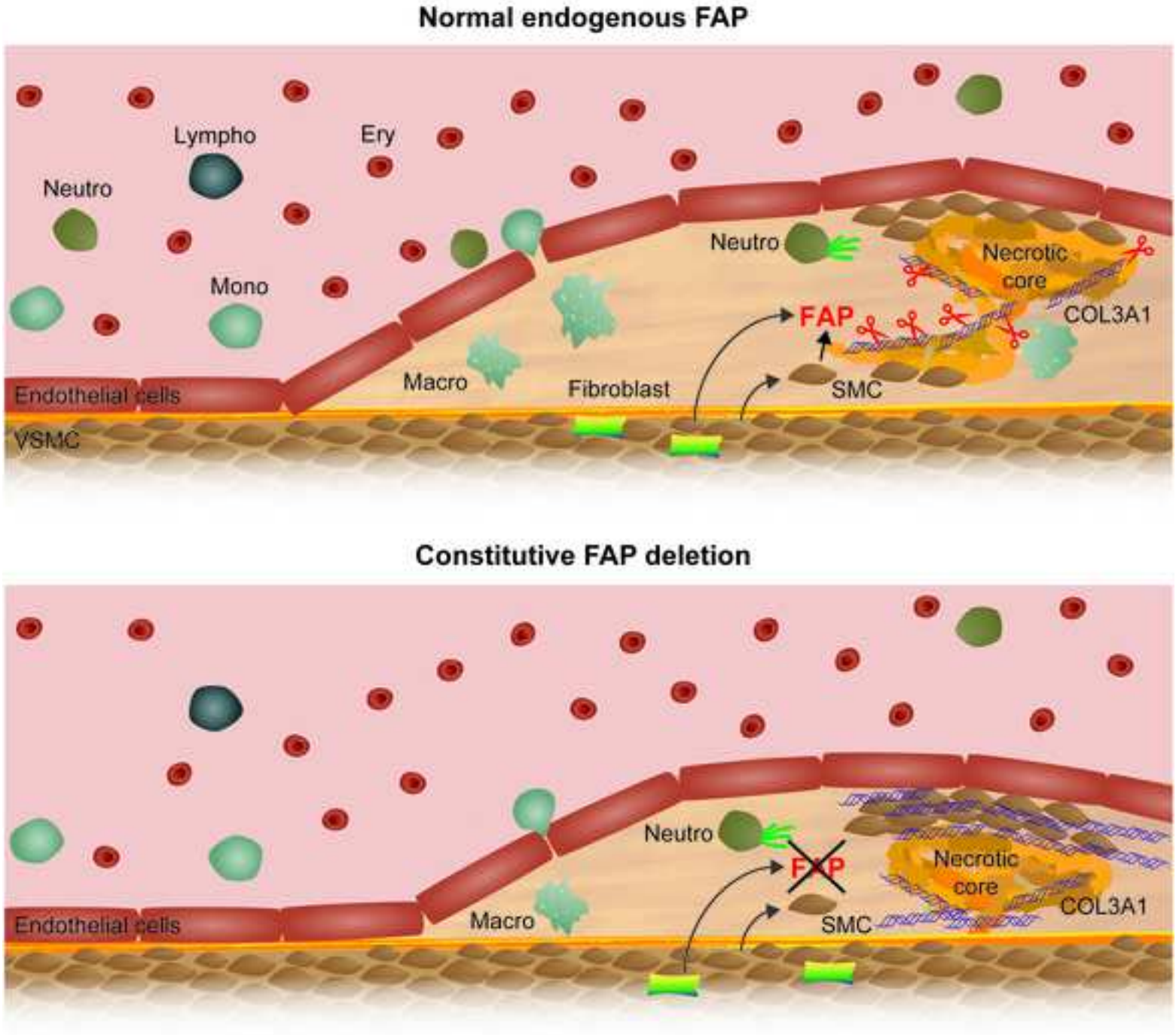

More pre-COL3A1, thicker fibrous caps, and less atherosclerotic lesions

Graphical Abstract

Normal endogenous FAP

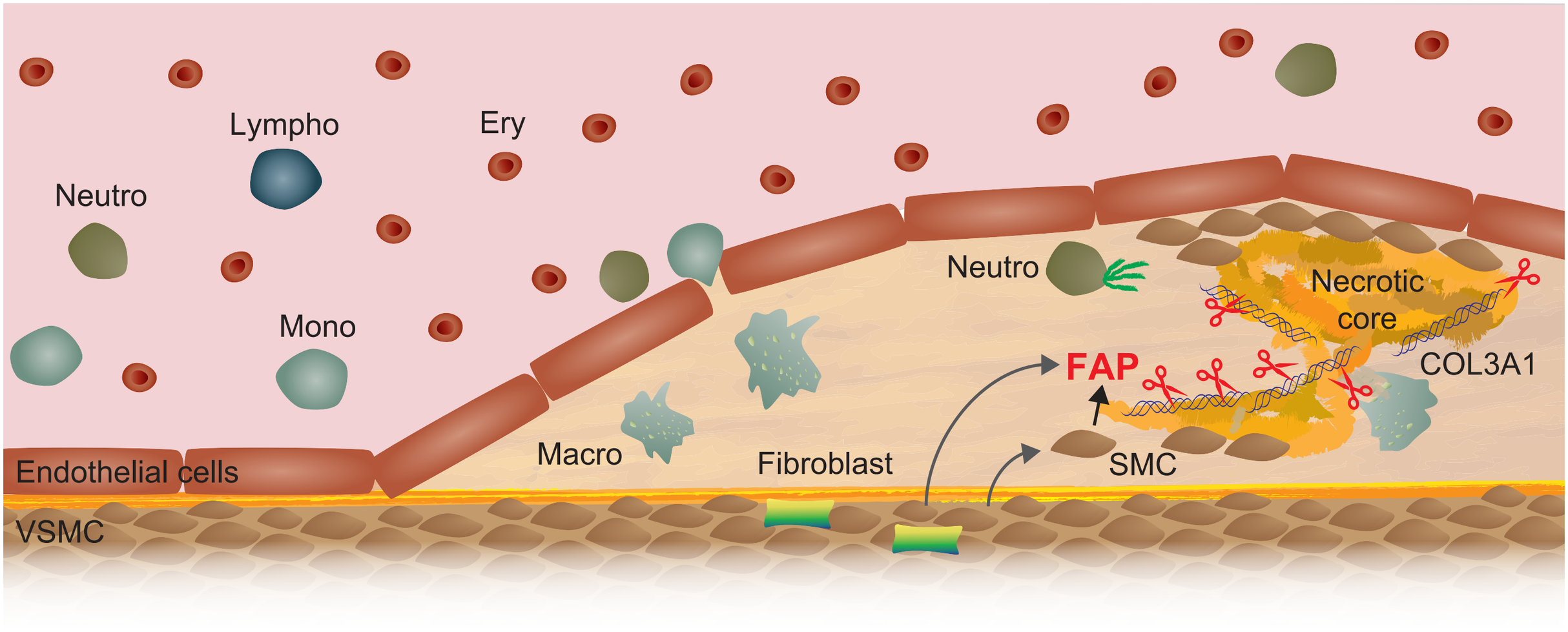

Constitutive FAP deletion

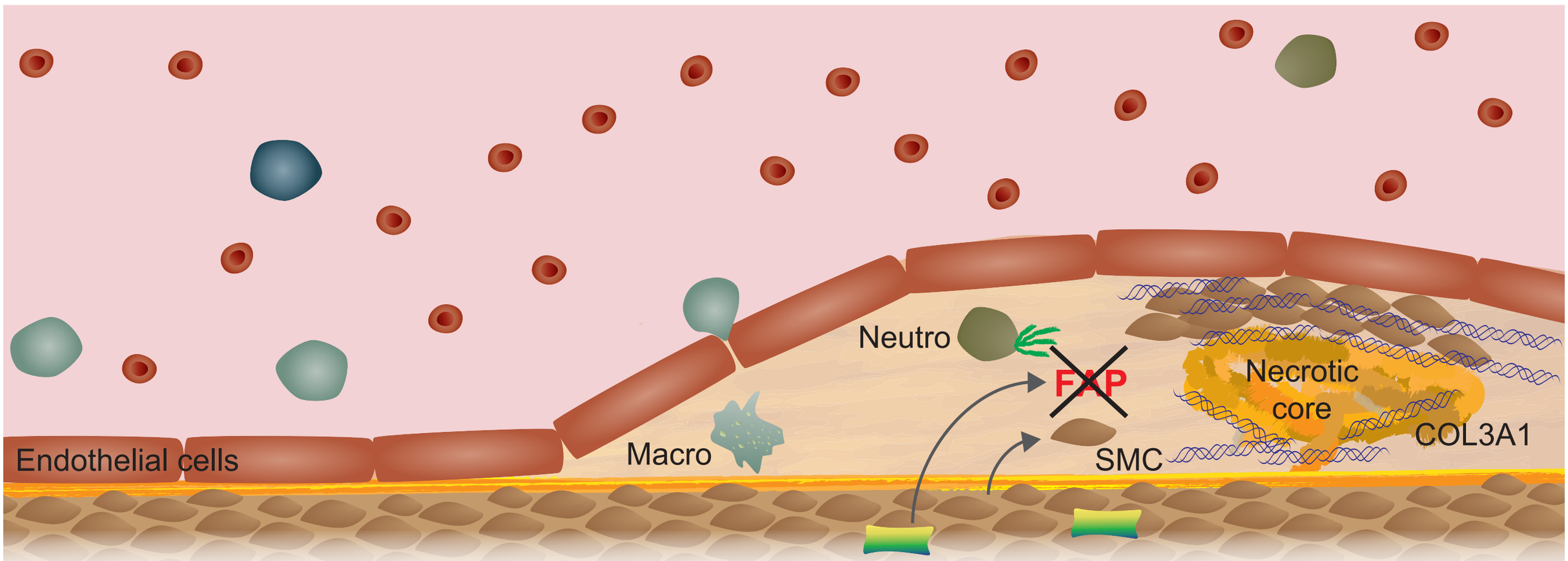

More pre-COL3A1, thicker fibrous caps, and less atherosclerotic lesions

Supplemental Information for

Deletion of fibroblast activation protein provides atheroprotection

Contact e-mail: sokrates.stein@uzh.ch and christian.matter@usz.ch

Figure S1

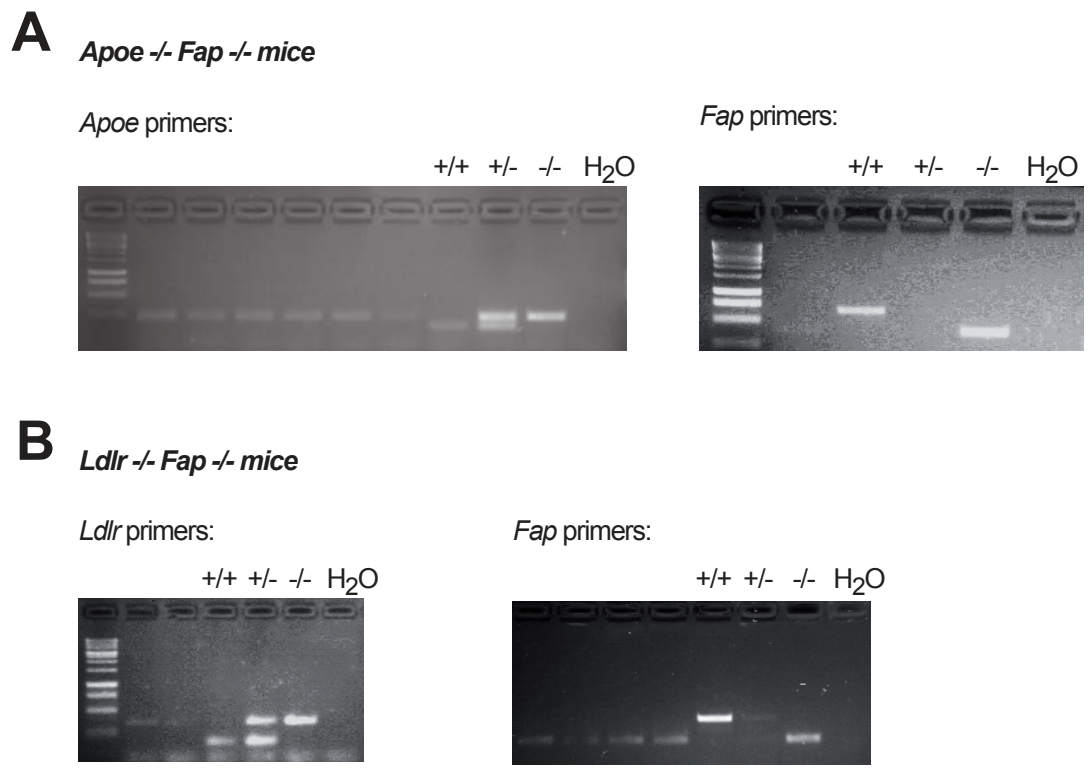

Figure S1. *Validation of the genotype of Apoe$^{-/-}$ Fap$^{-/-}$ and Ldlr$^{-/-}$ Fap$^{-/-}$ mice and the corresponding controls*. (**A, B**) PCR validation of (**A**) *Apoe$^{-/-}$ Fap$^{+/+}$* and *Apoe$^{-/-}$ Fap$^{-/-}$* mice and (**B**) *Ldlr$^{-/-}$ Fap$^{+/+}$* and *Ldlr$^{-/-}$ Fap$^{-/-}$* mice.

Figure S2

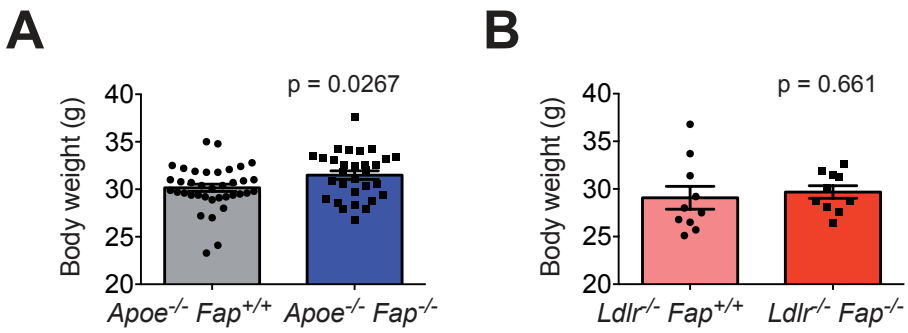

Figure S2. *Body weight of atherosclerotic mice lacking Fap*. (**A, B**) Body weight of (**A**) *Apoe*$^{-/-}$ *Fap*$^{+/+}$ and *Apoe*$^{-/-}$ *Fap*$^{-/-}$ mice *and* (**B**) *Ldlr*$^{-/-}$ *Fap*$^{+/+}$ and *Ldlr*$^{-/-}$ *Fap*$^{-/-}$ mice that were fed a high-cholesterol diet for 12 weeks. Data are represented in scatter plots and bars ± standard error; unpaired two-tailed Student's *t*-test.

Figure S3

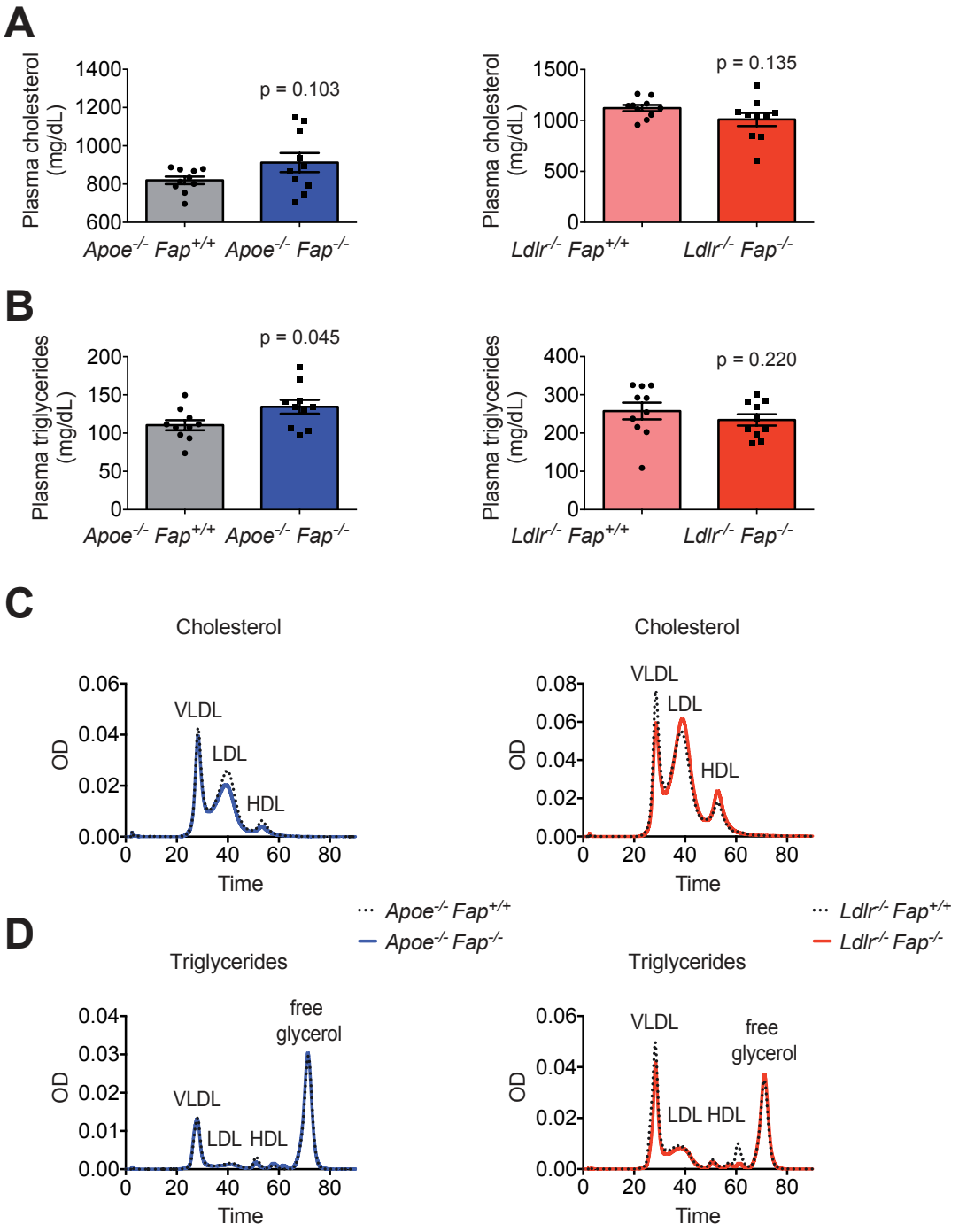

Figure S3. *Plasma lipid levels in atherosclerotic Fap-deficient mice*. (**A, B**) Total plasma cholesterol and (**B**) triglyceride levels in *Apoe*$^{-/-}$ *Fap*$^{+/+}$ versus *Apoe*$^{-/-}$ *Fap*$^{-/-}$ mice as well as in *Ldlr*$^{-/-}$ *Fap*$^{+/+}$ and *Ldlr*$^{-/-}$ *Fap*$^{-/-}$ mice. n = 10 per genotype. (**C, D**) Cholesterol and (**B**) triglycerides levels in lipoprotein subfractions of *Apoe*$^{-/-}$ *Fap*$^{+/+}$ versus *Apoe*$^{-/-}$ *Fap*$^{-/-}$ mice as well as in *Ldlr*$^{-/-}$ *Fap*$^{+/+}$ and *Ldlr*$^{-/-}$ *Fap*$^{-/-}$ mice. n = 1 pool from 10 mice per genotype. Data are represented in scatter plots and bars ± standard error (A and B) or plotting individual values on a XY graph. unpaired two-tailed Student's *t*-test (**A, B**).

Figure S4

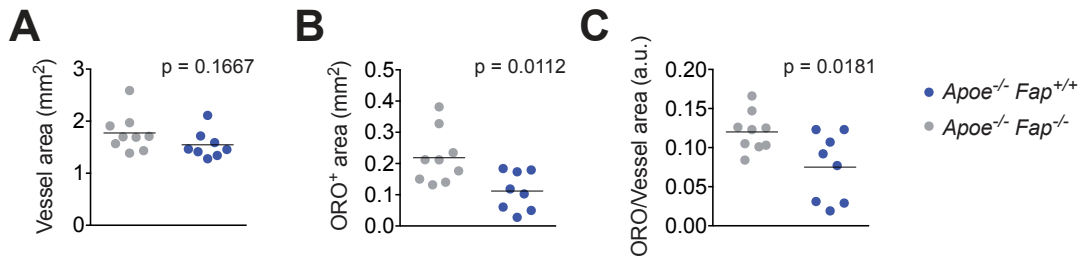

Figure S4. *Aortic sinus plaque analysis*. (**A**) Entire aortic sinus from *Apoe*$^{-/-}$ *Fap*$^{+/+}$ versus *Apoe*$^{-/-}$ *Fap*$^{-/-}$ mice. (**B**) Oil-red O-positive area in aortic sinus of *Apoe*$^{-/-}$ *Fap*$^{+/+}$ versus *Apoe*$^{-/-}$ *Fap*$^{-/-}$ mice. (**C**) Oil-red O-positive area relative to vessel area in aortic sinus of *Apoe*$^{-/-}$ *Fap*$^{+/+}$ versus *Apoe*$^{-/-}$ *Fap*$^{-/-}$ mice. n = 9 *Apoe*$^{-/-}$ *Fap*$^{+/+}$, n = 8 *Apoe*$^{-/-}$ *Fap*$^{-/-}$ mice. Data are represented in scatter plots with means; unpaired two-tailed Student's *t*-test.

Figure S5

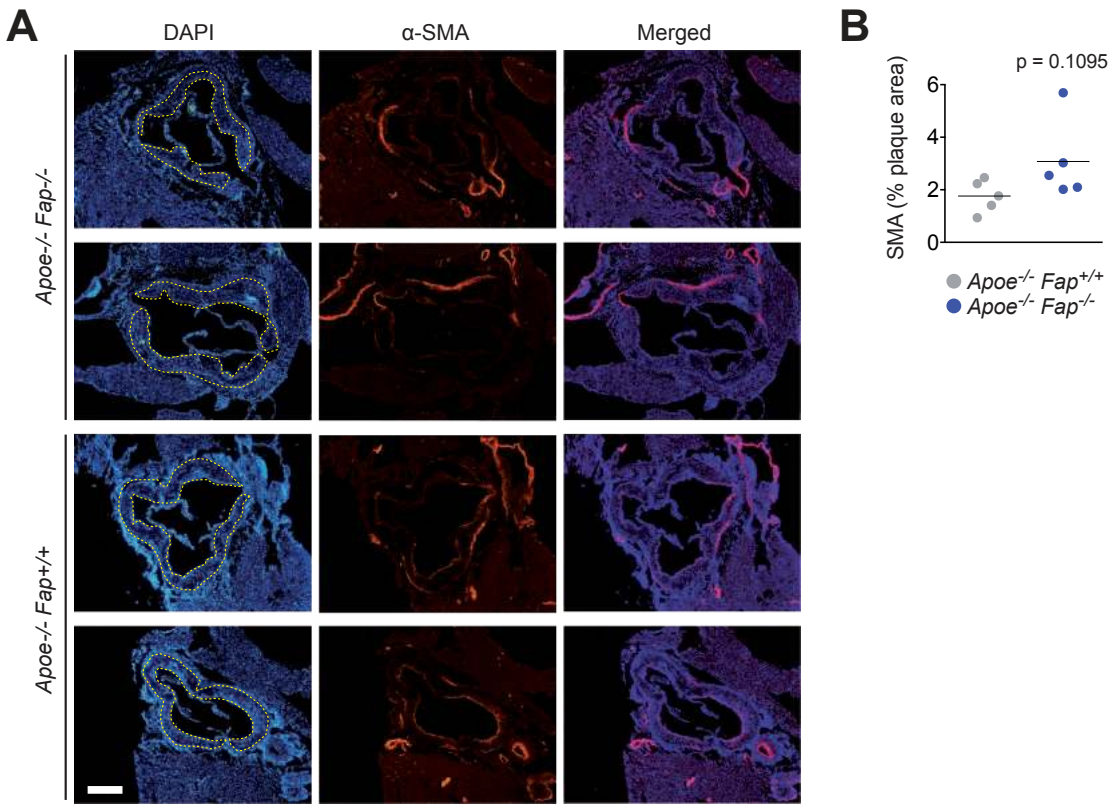

Figure S5. *Vascular smooth muscle cell staining*. (**A, B**) Representative images (**A**) and quantification (**B**) of intra-plaque α-smooth mucle actin (α-SMA) staining in cross-sections from the aortic sinus. The plaque area is marked in yellow dotted lines in the DAPI images. n ≥ 5 per genotype (4 cross-sections per mouse). White bar = 400 μm. Data are represented in scatter plots with means; unpaired two-tailed Student's *t*-test.

Figure S6

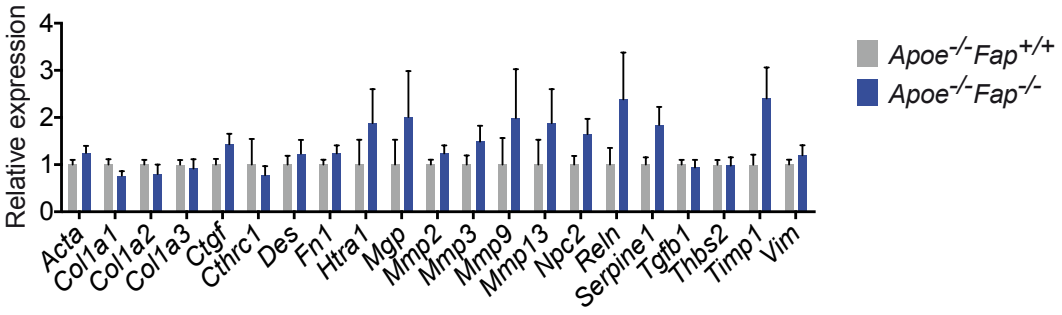

Figure S6. *Expression levels of extracellular matrix modulators*. mRNA expression of collagens, matrix metalloproteinases, and markers of fibrosis in aortae from *Apoe*$^{-/-}$ *Fap*$^{+/+}$ versus *Apoe*$^{-/-}$ *Fap*$^{-/-}$ mice. n = 6 per genotype. Data are represented in bar graphs with means and standard errors.

Figure S7

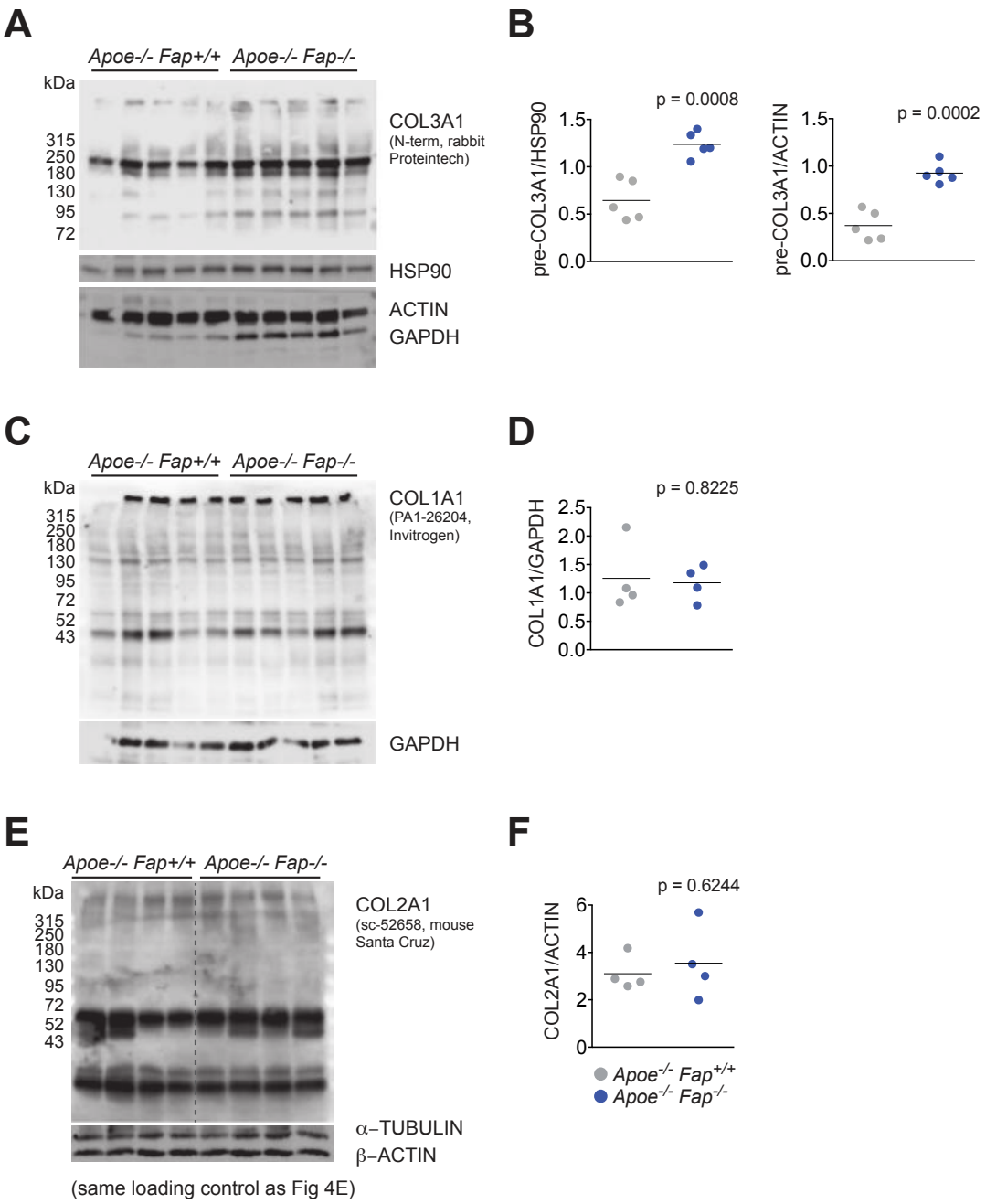

Figure S7. *COL13A1, COL1A1 and COL2A1 protein levels in atherosclerotic Fap-deficient mice*. (**A, B**) COL3A1 immunoblots (A) from aortae from *Apoe*$^{-/-}$ *Fap*$^{-/-}$ and *Apoe*$^{-/-}$ *Fap*$^{+/+}$ mice and their quantification (B). n = 5 per genotype (**C, D**) COL1A1 immunoblots (C) from aortae from *Apoe*$^{-/-}$ *Fap*$^{-/-}$ and *Apoe*$^{-/-}$ *Fap*$^{+/+}$ mice, respectively. n = 5 per genotype. (D) Quantification of COL1A1 expression (n = 4 per genotype; the two external lanes were excluded). (**E, F**) COL2A1 immunoblots (E) from aortae from *Apoe*$^{-/-}$ *Fap*$^{-/-}$ and *Apoe*$^{-/-}$ *Fap*$^{+/+}$ mice and their quantification (F). n = 4 per genotype. Data are represented in scatter plots with means; unpaired two-tailed Student's *t*-test.

Figure S8

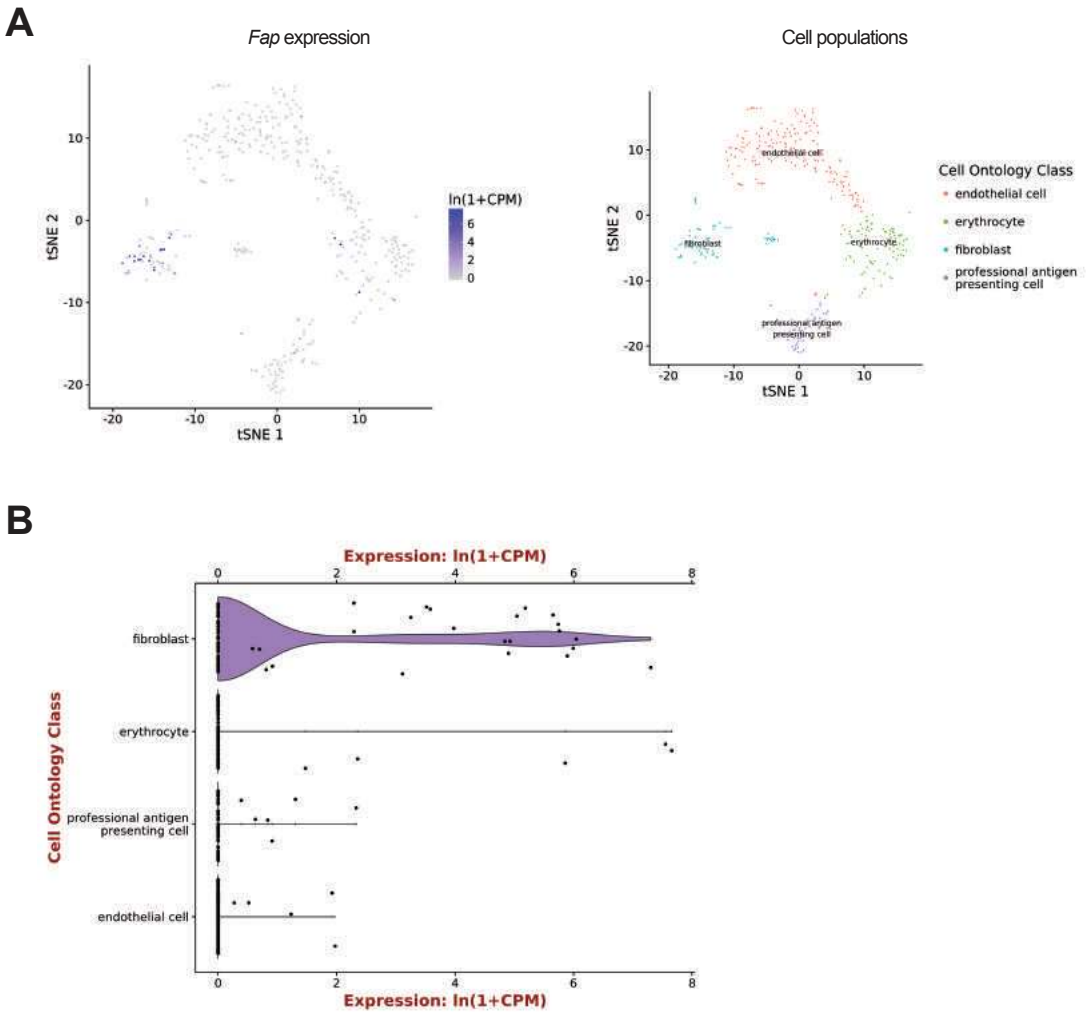

Figure S8. *Fap expression in aortae of 3-month-old C57BL/6JN mice*. (**A**) *Fap* expression in different aortic cell populations as described on the right panel. (**B**) Quantification of *Fap* expression in corresponding vascular cells. Graphs were directly exported from the *Tabula muris* dataset[24].

Table S1. Hematological analyses.

	WBC	RBC	PLT	Neutrophils		Lymphocytes		Monocytes		Eosinophils		Basophils	
	number 10*9/L	number 10*12/L	number $10^3/\mu L$	%	number $10^3/\mu L$	%	number 10e3/μL	%	number $10^3/\mu L$	%	number $10^3/\mu L$	%	number $10^3/\mu L$
Apoe$^{-/-}$ *Fap*$^{+/+}$ (n=10)	6.593 ± 0.5620	9.190 ± 0.1246	1891 ± 164.2	52.20 ± 2.401	3.502 ± 0.4123	39.18 ± 2.422	2.549 ± 0.2428	1.290 ± 0.2442	0.0790 ± 0.01130	2.790 ± 1.143	0.1630 ± 0.05727	0.4000 ± 0.06325	0.0260 ± 0.003712
Apoe$^{-/-}$ *Fap*$^{-/-}$ (n=12)	6.234 ± 0.7441	9.234 ± 0.2201	1480 ± 118.2	28.86 ± 1.881	1.694 ± 0.1213	61.47 ± 1.883	3.926 ± 0.6243	2.833 ± 0.2076	0.1767 ± 0.0255	3.700 ± 0.6370	0.2275 ± 0.04432	0.3750 ± 0.02787	0.02333 ± 0.002562
P value	0.7138	0.8704	0.0511	< 0.0001	0.0002	< 0.0001	0.0707	< 0.0001	0.0038	0.4760	0.3764	0.7051	0.5508
Ldlr$^{-/-}$ *Fap*$^{+/+}$ (n=9)	7.557 ± 0.9580	9.794 ± 0.1407	1208 ± 104.4	17.09 ± 1.656	1.199 ± 0.1184	74.19 ± 1.708	5.714 ± 0.8037	2.711 ± 0.4118	0.1967 ± 0.02867	2.422 ± 0.3800	0.1911 ± 0.03642	0.4667 ± 0.03333	0.03444 ± 0.005031
Ldlr$^{-/-}$ *Fap*$^{-/-}$ (n=10)	9.163 ± 0.4785	9.808 ± 0.09269	1414 ± 140.5	13.50 ± 0.7397	1.241 ± 0.09821	79.31 ± 1.316	7.252 ± 0.3676	2.750 ± 0.4342	0.2560 ± 0.04190	1.580 ± 0.4685	0.1442 ± 0.05537	0.4500 ± 0.03727	0.0420 ± 0.005121
P value	0.14	0.9356	0.2644	0.056	0.786	0.028	0.0894	0.9492	0.2691	0.1866	0.499	0.7452	0.3091

WBC, white blood cell; PLT, platelets; RBC, red blood cells; unpaired two-tailed Student's *t*-test.

Table S2. Selection of the highest transcripts in cells expressing *Fap* in atherosclerotic *Apoe* aortae.

CATCCAC AGATCCT GT-1	CCTACAC TCCAATG GT-1	GTATTCT CATGCTA GT-1	GTGCATA GTATCGC AT-1	CACACTC GTTTAGG AA-1	CCTTCGA TCCACTC CA-1	CTTGGCT GTCAAGC GA-1	GACGCGT GTATCTG CA-1	GCTCTGT AGCGTCA AG-1	GGACAAG GTAAATA CG-1	TGCCCTA CAAGCCG TC-1	TGGCGCA CAAGGAC TG-1	TGTGGTA AGGCGAC AT-1
Col3a1	*Dcn*	*Mgp*	*Gsn*	*Gsn*	*Dcn*	*Gsn*	*Gsn*	*Cytl1*	*Gsn*	*Dcn*	*Dcn*	*Gsn*
S100a6	*Gsn*	*Cst3*	*Dcn*	*S100a6*	*Gsn*	*Dcn*	*S100a6*	*Cst3*	*Dcn*	*Tmsb4x*	*Tmsb4x*	*Dcn*
Tmsb4x	*Rps27*	*Dcn*	*Tmsb4x*	*Dcn*	*Ftl1*	*Tmsb4x*	*Dcn*	*Rpl41*	*Mgp*	*Rpl41*	*Rpl41*	*Mfap5*
Col1a2	*Rpl41*	*Igfbp7*	*Rpl41*	*Ftl1*	*S100a6*	*B2m*	*Ftl1*	*Gsn*	*Igfbp7*	*S100a6*	*Gsn*	*S100a6*
Fn1	*Mfap5*	*Lum*	*Mfap5*	*Tmsb4x*	*Ifitm3*	*Ftl1*	*Cst3*	*3110079O 15Rik*	*Mt1*	*Mfap5*	*Ftl1*	*Rpl41*
Dcn	*Rps19*	*Rpl41*	*Rps27*	*Rpl41*	*Rpl41*	*S100a6*	*Col3a1*	*Mia*	*Ftl1*	*Col1a2*	*Cxcl1*	*Mt1*
Mfap5	*Ftl1*	*Cfh*	*Rpl37a*	*Mt1*	*B2m*	*Rpl41*	*Rpl41*	*Rps19*	*Rpl41*	*Rpl35*	*S100a6*	*Igfbp5*
Postn	*Rpl37a*	*Ftl1*	*Ftl1*	*Fn1*	*Penk*	*Ifitm3*	*Tmsb4x*	*Rpl37a*	*Hbb-bs*	*Ftl1*	*Rps27*	*Mt2*
Rpl41	*Rps3a1*	*Gsn*	*S100a6*	*Rpl35*	*Mt2*	*Tnfaip6*	*Rpl37a*	*Rps6*	*B2m*	*Tmsb10*	*Mt1*	*Tmsb4x*
Serpinh1	*Rpl35*	*Tmsb4x*	*Rpl35*	*Rps19*	*Tmsb4x*	*Rps27*	*B2m*	*Rps5*	*Ifitm3*	*Gsn*	*Rpl37a*	*Rps27*
Gsn	*Rpl32*	*Bgn*	*Rps19*	*Rpl37a*	*Rarres2*	*Rpl10*	*Igfbp7*	*Rps4x*	*Tmsb4x*	*Rps19*	*Rps19*	*Hbb-bs*
Vim	*S100a6*	*Hbb-bs*	*Rpl18a*	*Ubc*	*Rps27*	*Cxcl1*	*Rpl32*	*Rpl35*	*Rpl37a*	*Col3a1*	*Rps4x*	*Ftl1*
S100a10	*Hbb-bs*	*Rps27*	*Rpl10*	*Vim*	*Pcolce*	*Rpl37a*	*Hbb-bs*	*Rps11*	*Bgn*	*Mt2*	*Rps5*	*Rpl35*
Ftl1	*Rpl10*	*Rpl37a*	*Rps8*	*Rps27*	*Col1a2*	*S100a9*	*Ifitm2*	*Wif1*	*Jund*	*Rpl37a*	*Mfap5*	*S100a8*
Serf2	*Serping1*	*Vim*	*Igfbp5*	*Rpl18a*	*Lum*	*Rps19*	*Rps27*	*Rplp0*	*Junb*	*Rps27*	*Cst3*	*S100a11*
Tppp3	*Rps8*	*Rps5*	*Rps15a*	*Rps5*	*Plac8*	*Tmsb10*	*Ifitm3*	*Rpl18a*	*Mt2*	*S100a11*	*Rpl18a*	*Rpl18a*
Cxcl2	*Mt2*	*Rplp0*	*Vim*	*Dpt*	*Tmsb10*	*Rpl35*	*Rpl35*	*Vim*	*Rps27*	*Rpl18a*	*Rpl10*	*Tmsb10*
Cd63	*Rps9*	*Rpl13a*	*Rpl32*	*Rpl32*	*S100a9*	*Hbb-bs*	*Rpl10*	*Rps27*	*Rps19*	*Rpl10*	*Vim*	*Rpl37a*
Hbb-bs	*Rpl18a*	*S100a8*	*Rpl9*	*Pcolce*	*Rps4x*	*Rpl13a*	*Rps4x*	*Rpl13a*	*Cst3*	*Igfbp5*	*Rps8*	*Rps19*
Cxcl1	*B2m*	*Cytl1*	*Rps3*	*Tppp3*	*Gstm1*	*Serpinh1*	*Col6a2*	*Rpl32*	*S100a6*	*Hbb-bs*	*Hbb-bs*	*Dpt*

Top 20 transcripts for each cell with a Fap sequencing count > 2. Original data from [1].

Table S3. Pathway analyses of the selected transcripts from table S2.

Top 10 GOTERM_BP Term	P Value	Fold Enrichment	Bonferroni	Benjamini	FDR
GO:0006412~translation	3.99E-15	12.599311	1.90E-12	1.90E-12	5.72E-12
GO:0032496~response to lipopolysaccharide	8.19E-06	10.798447	0.003885	0.001944	0.011715
GO:0030199~collagen fibril organization	1.28E-05	34.091252	0.006081	0.002031	0.018358
GO:0007568~aging	4.33E-05	10.759436	0.020352	0.005127	0.061869
GO:0009612~response to mechanical stimulus	8.70E-05	21.104108	0.040482	0.008231	0.124299
GO:0009314~response to radiation	1.84E-04	35.454902	0.083596	0.014444	0.262405
GO:0042060~wound healing	4.09E-04	14.144243	0.176457	0.027353	0.582618
GO:0043206~extracellular fibril organization	7.28E-04	72.521390	0.292442	0.042320	1.035793
GO:0001649~osteoblast differentiation	8.19E-04	11.766007	0.322242	0.042298	1.163880
GO:0042989~sequestering of actin monomers	8.72E-04	66.477941	0.339104	0.040570	1.238798

Top 10 GOTERM_CC Term	P Value	Fold Enrichment	Bonferroni	Benjamini	FDR
GO:0005840~ribosome	2.15E-21	28.38738602	2.57E-19	2.57E-19	2.46E-18
GO:0031012~extracellular matrix	9.45E-21	20.06326531	1.13E-18	5.67E-19	1.08E-17
GO:0070062~extracellular exosome	5.39E-16	4.09668768	6.66E-14	2.22E-14	6.33E-13
GO:0022627~cytosolic small ribosomal subunit	2.45E-15	58.29703504	2.93E-13	7.33E-14	2.81E-12
GO:0005576~extracellular region	1.99E-13	4.806943199	2.38E-11	4.77E-12	2.28E-10
GO:0030529~intracellular ribonucleoprotein complex	4.76E-12	13.16651786	5.71E-10	9.52E-11	5.47E-09
GO:0005925~focal adhesion	6.88E-11	10.77566679	8.25E-09	1.18E-09	7.90E-08
GO:0005615~extracellular space	1.07E-10	4.668977964	1.29E-08	1.61E-09	1.23E-07
GO:0022625~cytosolic large ribosomal subunit	3.07E-08	24.69324961	3.69E-06	4.10E-07	3.53E-05
GO:0005578~proteinaceous extracellular matrix	1.55E-06	8.888788427	1.86E-04	1.86E-05	0.001782
GO:0015935~small ribosomal subunit	3.09E-06	48.42857143	3.70E-04	3.37E-05	0.003544

Top 10 GOTERM_MF Term	P Value	Fold Enrichment	Bonferroni	Benjamini	FDR

GO:0003735~structural constituent of ribosome	4.48E-20	20.651042	5.82E-18	5.82E-18	5.21E-17
GO:0044822~poly(A) RNA binding	6.98E-09	4.898360	9.08E-07	4.54E-07	8.13E-06
GO:0019843~rRNA binding	2.67E-05	28.395182	0.003461	0.001155	0.031050
GO:0003729~mRNA binding	1.60E-04	11.518046	0.020602	0.005191	0.186307
GO:0005518~collagen binding	0.001263	18.480932	0.151523	0.032328	1.461140
GO:0005201~extracellular matrix structural constituent	0.009613	19.945884	0.715115	0.188831	10.638815
GO:0008201~heparin binding	0.017288	7.221026	0.896388	0.276657	18.379381
GO:0035662~Toll-like receptor 4 binding	0.017928	109.037500	0.904799	0.254701	18.996059
GO:0048306~calcium-dependent protein binding	0.025784	11.851902	0.966489	0.314303	26.228997
GO:0050786~RAGE receptor binding	0.028532	68.148438	0.976789	0.313613	28.616601

Top 10 UP_KEYWORDS Term	**P Value**	**Fold Enrichment**	**Bonferroni**	**Benjamini**	**FDR**
Ribosomal protein	2.15E-23	31.471588	2.50E-21	2.50E-21	2.46E-20
Ribonucleoprotein	6.32E-20	20.742638	7.33E-18	3.66E-18	7.21E-17
Secreted	2.12E-13	5.308146	2.46E-11	8.21E-12	2.42E-10
Extracellular matrix	4.44E-08	13.593048	5.15E-06	1.29E-06	5.06E-05
Acetylation	8.75E-07	2.759932	1.01E-04	2.03E-05	9.98E-04
Disulfide bond	3.23E-06	2.658563	3.74E-04	6.24E-05	0.003683
Signal	9.87E-05	2.039107	0.011380	0.001634	0.112503
Chemotaxis	2.06E-04	16.991310	0.023592	0.002980	0.234539
Pyrrolidone carboxylic acid	8.09E-04	21.656720	0.089582	0.010374	0.918799
Innate immunity	8.97E-04	7.952779	0.098838	0.010353	1.018331

Top 10 terms as indicated in the column titles: BP, biological process; CC, cellular component; MF, molecular function; UP, UniProtKB keywords.

Table S4. Primers used for qPCR.

Transcript	Forward (5' to 3')	Reverse(5' to 3')
Acta	CCAGAGCAAGAGAGGGATCCT	TGTCGTCCCAGTTGGTGATG
Actb	TGTTACCAACTGGGACGACA	GGGGTGTTGAAGGTCTCAAA
B2m	TTCTGGTGCTTGTCTCACTG	TATGTTCGGCTTCCCATTCT
Col1a1	GCACGAGTCACACCGGAACT	AAGGGAGCCACATCGATGAT
Col1a2	CTACTGGTGAAACCTGCATCCA	GGGCGCGGCTGTATGAG
Col3a1	TCCTGAAGATGTCGTTGATGTG	TTTTTGCAGTGGTATGTAATGTTCTG
Ctgf	CACTCTGCCAGTGGAGTTCA	AAGATGTCATTGTCCCCAGG
Cthrc1	CGGGATGGATTCAAAGGGGA	CGTGAATGTACACTCCGCAAT
Des	CTCGGAAGTTGAGAGCAGAGA	GTGAAGATGGCCTTGGATGT
Fn1	ACTGGATGGGGTGGGAAT	GGAGTGGCACTGTCAACCTC
Fn1	ACTGGATGGGGTGGGAAT	GGAGTGGCACTGTCAACCTC
Gfap	CCTTCTGACACGGATTTGGT	ACATCGAGATCGCCACCTAC
Htra1	GATCTTCCTGCCCTTGGC	CTACACCAACCTGTGCCAGC
Mgp	AGGACTCCATGCTTTCGTGA	ACCCGAGACACCATGAAGAG
Mgp	AGGACTCCATGCTTTCGTGA	ACCCGAGACACCATGAAGAG
Mmp13	TTGCCCTGGGAAGGAGAGA	AGTCCAGCTCAACAAGAAGAAGGT
Mmp14	AGTCAGGGTCACCCACAAAGA	TTTGGGCTTATCTGGGACAGA
Mmp2	ACCACCTTAACTGTTGCTTTTG	AGGAAATGCAGTGGAGTGGAA
Mmp3	GGAGCTAGCAGGTTATCCTAAAAGC	TAGAAATGGCAGCATCGATCTTC
Mmp7	GGTGAGGACGCAGGAGTGAA	GAAGAGTGACTCAGACCCAGA
Mmp8	AAAAGGGAAGCTCAGTCTGTATACTC	AGAGGGCTGCAGAGTTAGTTACCA
Mmp9	GGACGACGTGGGCTACGT	CACGGTTGAAGCAAAGAAGGA
Npc2	TTGTGCAGCTGACAGGGAT	CCCCTGCACTTCAAGGACT
Npc2	TTGTGCAGCTGACAGGGAT	CCCCTGCACTTCAAGGACT
Ppib	CAGGGGAGATGGCACAGGAG	CGGCTGTCTGTCTTGGTGCTCTCC
Reln	ACATGAGAGGCCACCACACT	CTTCTCAGAGCATTGGAGGC
Serpine1	TTGTCCAGCGGGACCTAGAG	AAGTCCACCTGTTTCACCATAGTCT
Tgfb1	CAACCCAGGTCCTTCCTAAA	GGAGAGCCCTGGATACCAAC
Tgfb1	CAACCCAGGTCCTTCCTAAA	GGAGAGCCCTGGATACCAAC
Thbs2	AGTGCACAGCTACAGCCTGA	ACAGAGTACTGGCGTCGGTC
Thbs2	AGTGCACAGCTACAGCCTGA	ACAGAGTACTGGCGTCGGTC
Timp1	CCTTCGCATGGACATTATTCTC	TCTCTAGGAGCCCCGATCTG
Vim	GGATTCCACTTTCCGTTCAA	GAAATTGCAGGAGGAGATGC

Supplementary References

1. Gu W, Ni Z, Tan YQ, Deng J, Zhang SJ, Lv ZC, Wang XJ, Chen T, Zhang Z, Hu Y, Jing ZC, Xu Q. Adventitial Cell Atlas of wt (Wild Type) and ApoE (Apolipoprotein E)-Deficient Mice Defined by Single-Cell RNA Sequencing. *Arterioscler Thromb Vasc Biol* 2019;**39**:1055-1071.

Full uncut blots

Figure 4E

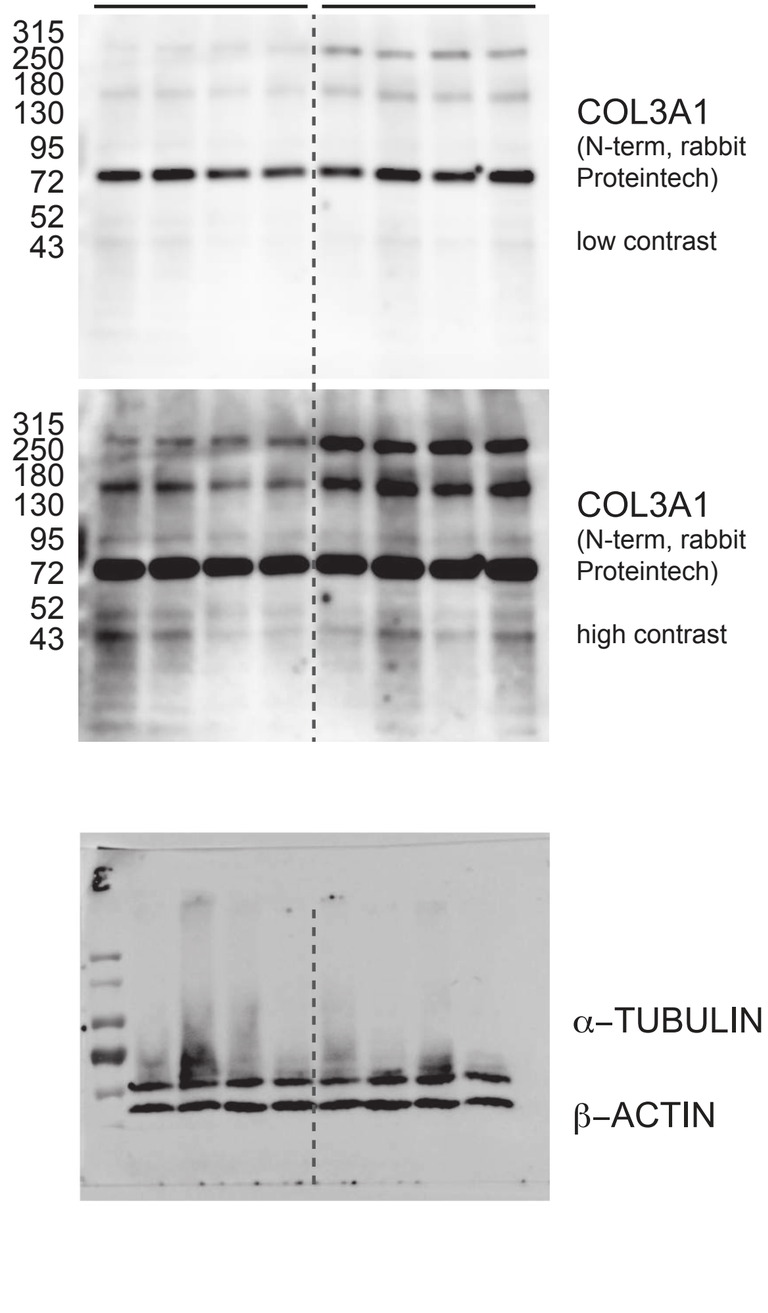

Figure S7A

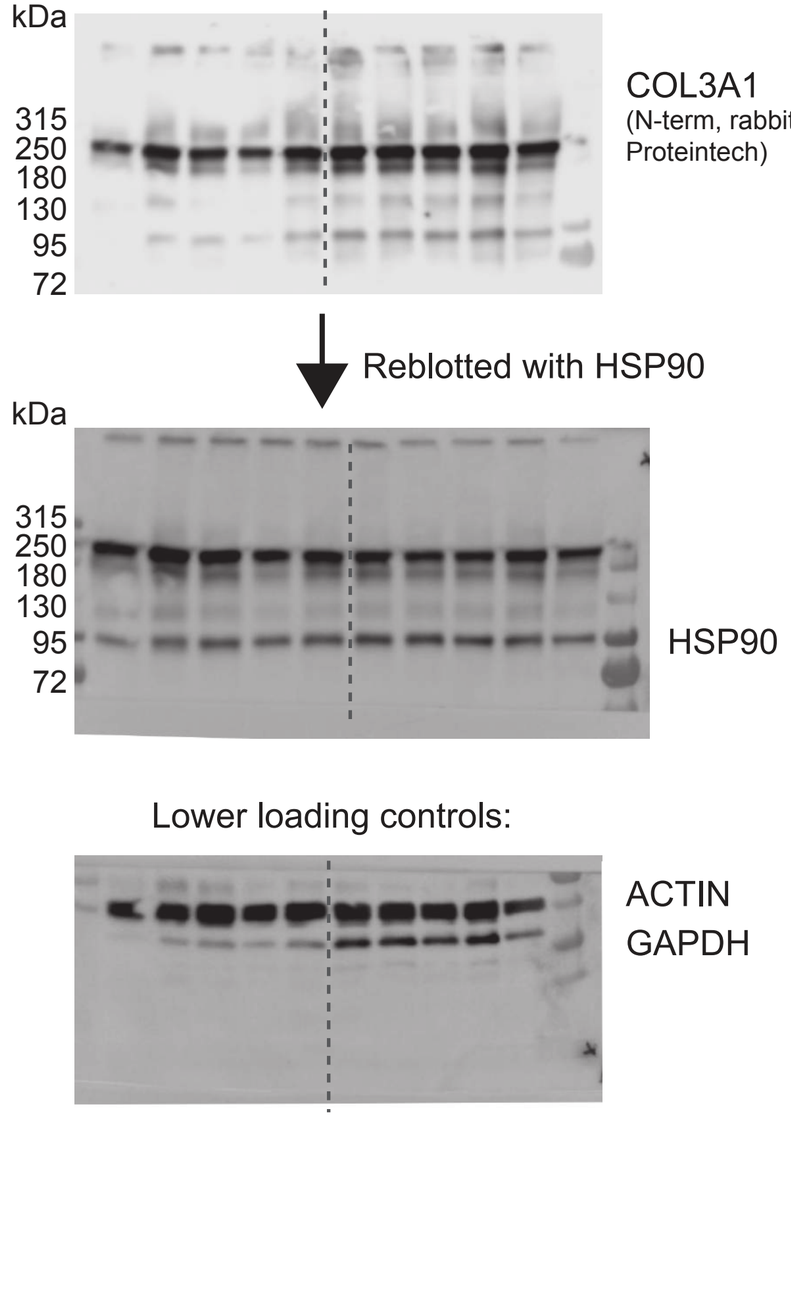

Figure S7C & E